CLUSTERING 24-HOUR AMBULATORY BLOOD PRESSURE TIME SERIES WITH DYNAMIC TIME WARPING AND TIME WARP EDIT DISTANCE

A Thesis

by

JOHN KNIGHT

Submitted in Partial Fulfillment of the

Requirements for the Degree of

MASTER OF SCIENCE

Major Subject: Applied Statistics and Data Science

The University of Texas Rio Grande Valley
December 2025

CLUSTERING 24-HOUR AMBULATORY BLOOD PRESSURE TIME SERIES WITH DYNAMIC TIME WARPING AND TIME WARP EDIT DISTANCE

A Thesis
by
JOHN KNIGHT

COMMITTEE MEMBERS

Dr. Kristina Vatcheva
Committee Chair

Dr. Yifeng Gao
Committee Member

Dr. Thoa Thieu
Committee Member

December 2025

Copyright John Knight 2025
All Rights Reserved

ABSTRACT

Knight, John, Clustering 24-Hour Ambulatory Blood Pressure Time Series with Dynamic Time Warping and Time Warp Edit Distance. Master of Science (MS), December 2025, 73 pp., 11 tables, 13 figures, 81 references.

Ambulatory blood pressure monitoring (ABPM) captures dynamic circadian changes in blood pressure (BP) that are not reflected in static clinic readings. This study applied time-series clustering with two elastic distance measures—Dynamic Time Warping (DTW) and Time Warp Edit Distance (TWED)—to identify distinct phenotypes in 2,155 24-hour ABPM time series from participants in the Maracaibo Aging Study. DTW and TWED both yielded three clusters corresponding to non-dipping, moderate-dipping, and strong-dipping patterns. The non-dipping group showed elevated nighttime BP, associated with greater cardiovascular and cognitive risk, while the strong-dipping group was associated with higher education and younger age in baseline clinic measurements. TWED indicated greater variability in non-dippers, whereas DTW results were more mixed. The TWED method was preferred overall for its clinically interpretable clusters and greater flexibility in handling irregular data. Results demonstrated that unsupervised time-series methods can capture clinically meaningful BP phenotypes beyond conventional summary metrics, supporting the use of elastic distance clustering for precision risk stratification in hypertension and aging research.

DEDICATION

To my parents, my brother, my wife, and my three daughters. You made this possible, and you made it worthwhile. Thanks for all the love and support.

ACKNOWLEDGMENTS

I owe a huge debt of gratitude to Dr. Kristina Vatcheva, chair of my thesis committee, for her continual support, thoughtful feedback, and mentorship. Her expertise and patience have greatly contributed to my growth as a researcher and to the completion of this thesis. Thanks also to Dr. Yifeng Gao and Dr. Thoa Thieu for serving on my thesis committee, and to Jennifer Mittelstaedt for her help with formatting and preparing the final manuscript.

I would also like to express my appreciation to Dr. Gladys Maestre, the PI of the Maracaibo Aging Study, for giving me access to the blood pressure time-series data on which this thesis was based.

TABLE OF CONTENTS

Page

ABSTRACT iii

DEDICATION iv

ACKNOWLEDGMENTS v

LIST OF TABLES vii

LIST OF FIGURES viii

CHAPTER I: INTRODUCTION 1

CHAPTER II: THEORETICAL BACKGROUND 11

Clustering and Distance Measures 11
Dynamic Time Warping 12
Time Warp Edit Distance 17
Partitional Clustering Methods for Time Series 19
Cluster Validation Indices 20

CHAPTER III: METHODS 23

Study Data 23
Data Analysis 24

CHAPTER IV: RESULTS 27

Descriptive Statistics 27
DTW-Derived Clusters 29
TWED-Derived Clusters 43

CHAPTER V: DISCUSSION 58

Conclusions 62

REFERENCES 64

VITA 73

LIST OF TABLES

Page

Table 1: AHA hypertension thresholds 26

Table 2: Summary of patient baseline socio-demographic and clinical characteristics..... 28

Table 3: Summary of ambulatory blood pressure statistics 28

Table 4: Comparison of ABP descriptive statistics across DTW-derived clusters..... 30

Table 5: Characterization of DTW-derived clusters 39

Table 6: Comparison of baseline socio-demographic and clinical characteristics between DTW-derived clusters..... 41

Table 7: Comparison of ABP descriptive statistics across TWED-derived clusters..... 44

Table 8: Characterization of TWED-derived clusters..... 53

Table 9: Comparison of baseline socio-demographic and clinical characteristics between TWED-derived clusters 54

Table 10: Comparison of DTW and TWED cluster membership among baseline patients..... 56

Table 11: Comparison of DTW and TWED cluster membership among all ABPM time series. 57

LIST OF FIGURES

Page

Figure 1: Example of a 24-hour ABPM time series from Maracaibo Aging Study data 2

Figure 2: Comparison of Euclidean matching and DTW matching..... 8

Figure 3: Visualization of the LB_Keogh lower bound for DTW 16

Figure 4: Histograms of nighttime mean DBP, MAP and SBP for DTW-derived clusters..... 34

Figure 5: Radar chart showing standardized values for significantly different continuous ABP variables across DTW-derived clusters..... 35

Figure 6: Loess-smoothed series means for DTW-derived clusters 36

Figure 7: Multidimensional scaling (3D) representation of DTW-derived clusters 37

Figure 8: Histograms of DBP, MAP and SBP dipping % for DTW-derived clusters..... 38

Figure 9: Histograms of nighttime mean DBP, MAP and SBP for TWED-derived clusters..... 48

Figure 10: Radar chart showing standardized values for significantly different continuous ABP variables across TWED-derived clusters 49

Figure 11: Loess-smoothed series means for TWED-derived clusters..... 50

Figure 12: Multidimensional scaling (3D) representation of TWED-derived clusters..... 51

Figure 13: Histograms of DBP, MAP and SBP dipping % for TWED-derived clusters 52

CHAPTER I

INTRODUCTION

Blood pressure (BP) is a critical physiological measure used to assess cardiovascular health and is routinely recorded during clinical encounters due to its ease of measurement and non-invasive nature. Commonly reported measures are systolic blood pressure (SBP), representing the maximum pressure in the arteries during heart contractions, and diastolic blood pressure (DBP), representing the minimum pressure when the heart is at rest. Mean arterial pressure (MAP), a weighted average of SBP and DBP, provides an overall indication of blood flow and organ perfusion. However, clinic-based BP readings provide only a brief snapshot of a patient's cardiovascular state, and can be influenced by various factors including recent food or drink intake, the patient's posture, or even talking during the procedure (Schutte et al., 2022). Clinic-based readings may also fail to capture important fluctuations throughout the day and night, such as masked hypertension (normal clinic readings but elevated out-of-clinic BP) or nocturnal BP surges, that carry independent prognostic significance (Asayama et al., 2023; Chia et al., 2022; Spatz et al., 2019, Staplin et al., 2023).

In response to growing awareness of the limitations of office-based readings, ambulatory blood pressure monitoring (ABPM) has emerged as a valuable tool for capturing dynamic BP patterns (Huang et al., 2021; Yang et al., 2019). ABPM involves measuring BP at regular intervals over a 24-hour period while the patient goes about their daily activities (Cleveland Clinic, 2023). This approach provides a more comprehensive assessment than single, in-clinic

measurements by capturing natural variations in BP across different times and contexts, and allows for the calculation of distinct BP metrics based on 24-hour, daytime, and nighttime periods. An example of a single patient's 24-hour ABPM measurements for SBP, DBP, and MAP can be seen in Figure 1.

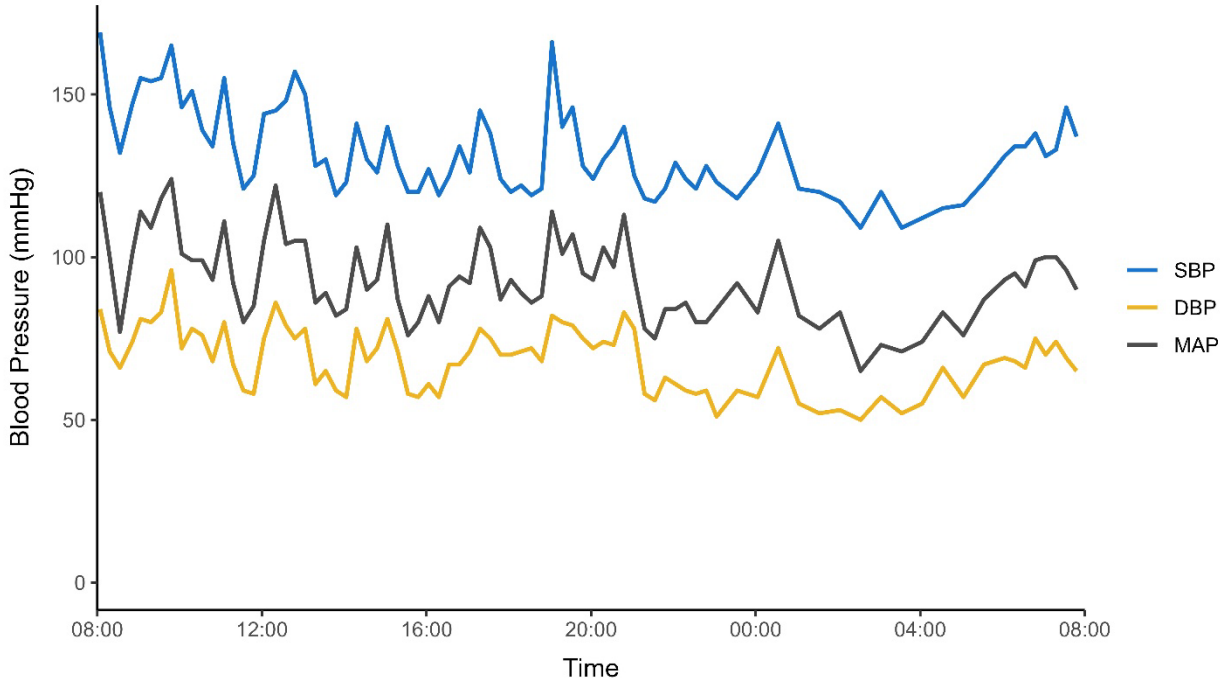

Figure 1: Example of a 24-hour ABPM time series from Maracaibo Aging Study data. Abbreviations: DBP, diastolic blood pressure; MAP, mean arterial pressure; SBP, systolic blood pressure.

Typically, daytime BP is higher due to physical and mental activity, while nighttime BP is lower during sleep, with 24-hour averages somewhere in between (Huang et al., 2021). Diagnostic thresholds for ambulatory hypertension differ from those used in office settings; for instance, based on the 2017 American Heart Association guidelines, a 24-hour average BP of ≥125/75 mmHg is considered hypertensive, compared to a clinic measurement of ≥130/80

mmHg (Huang et al., 2021; Manta et al., 2024; Whelton et al., 2018). ABPM also facilitates the analysis of BP variability and circadian patterns such as dipping and rising, which may provide further insight into cardiovascular risk beyond static BP values (Asmuje et al., 2022; Sible & Nation, 2024).

The timing and trajectory of BP changes during sleep may reflect distinct pathophysiological processes, independent of overall BP levels. For example, in a nationwide cohort of over 6,000 individuals with cardiovascular risk factors, Kario et al. (2020) found that both elevated nighttime systolic BP and a "riser" circadian pattern, characterized by an increase in BP during sleep, were strongly linked to a higher risk of cardiovascular events, particularly heart failure. The riser pattern was associated with more than twice the risk of heart failure compared to the typical "dipper" pattern, and this risk remained significant even after accounting for average nighttime BP. Additionally, other studies have found that high nighttime BP and high overall BP variability are associated with adverse cardiovascular and cognitive health outcomes (Melgarejo et al., 2024; Sible & Nation, 2024; Staplin et al., 2023; Sun, 2023; Yang et al., 2019).

Based on the literature review, analysis of 24-hour ABP has most frequently been conducted using various summary statistics. The most common measures of overall BP level and variability are the 24-hour mean and standard deviation (SD). Additional indices used to quantify overall BP variation include the coefficient of variation (COV) and variability independent of the mean (VIM), while short-term fluctuations between consecutive BP readings are captured by average real variability (ARV) (Sible & Nation, 2024; Sun, 2023; Zhu et al., 2020). These metrics can be derived over the full 24-hour period or separately for daytime and nighttime intervals. Another widely used measure is the ratio between daytime and nighttime BP, or "dipping" ratio, which reflects the expected circadian decline in BP during sleep. Numerous

studies have established the clinical relevance of this phenomenon, with non-dipping and "reverse dipping" profiles (i.e., higher nighttime BP) being associated with increased cardiovascular and cognitive risk (Gavriilaki et al., 2023; Sun, 2023; Xu et al., 2021).

While these conventional summary metrics have advanced our understanding of 24-hour ABP, they have some limitations. For example, two individuals may have identical 24-hour means and SDs, yet one may experience abrupt morning surges or episodic spikes that a single SD or ARV value cannot fully describe. Likewise, such metrics do not account for the temporal ordering of measurements, which may be clinically relevant; for instance in distinguishing sustained hypertension from intermittent surges. Furthermore, the nighttime dipping ratio is restricted to a predefined "nighttime" window, which may not align with an individual's actual sleep patterns. These derived metrics are nonetheless widely used as input features in predictive modeling frameworks such as regression and machine learning techniques (Asmuje et al., 2022; Melgarejo et al., 2024; Mena et al., 2017; Sible & Nation, 2024; Yang et al., 2019). Such methods represent *supervised* learning approaches, which rely on predefined outcome variables for model training.

A possible alternative approach to analyzing 24-hour ABP data is to employ *unsupervised* learning techniques such as clustering. Clustering analysis can uncover latent patterns or associations in data without the need for predefined categories or outcome labels. Clustering analysis has been widely applied in medical research to identify meaningful subgroups within patient populations. For example, Scherzer et al. (2018) applied unsupervised k-means clustering to serum biomarker data from 332 HIV-infected individuals to identify distinct phenotypic subgroups associated with cardiopulmonary abnormalities and mortality risk. The study identified three clusters: one characterized by elevated inflammatory markers, another

with high cardiac biomarkers, and a third with lower levels of both. The inflammatory and cardiac clusters were linked to significantly increased risks of diastolic dysfunction, pulmonary hypertension, and all-cause mortality, independent of traditional cardiovascular and HIV-related risk factors.

Similarly, Pallares Robles et al. (2023) used hierarchical clustering on clinical and molecular data from 591 patients with acute venous thromboembolism (VTE) to define distinct subgroups, or endotypes, based on 58 clinical variables. The study identified four endotypes with varying prognoses: one group of older individuals with comorbidities faced the highest risk of thromboembolic events or death, while another consisting of men with a history of VTE and provoking risk factors also had significantly elevated risk. Each endotype exhibited distinct molecular profiles, reinforcing differences in underlying pathophysiology and highlighting the limitations of traditional VTE classifications. Studies such as these illustrate how clustering analysis can reveal clinically relevant patient subgroups that may be overlooked by supervised statistical methods, offering deeper insights into disease progression and risk stratification that support more precise and personalized medical care (Moore et al., 2010; Vargas, 2023).

Clustering has been used in relatively few studies to analyze BP data. Early work by Rodríguez et al. (1992) applied *k*-means clustering to cosinor model parameters to classify circadian BP rhythms into clinically meaningful subtypes. More recently, several studies have extended clustering directly to 24-hour ABPM time series. Guo et al. (2017) applied *k*-means clustering to ABPM and clinical data from over 500 hypertensive patients, identifying four subgroups with distinct cardiovascular risk profiles, including a reverse-dipping cluster strongly associated with coronary artery disease. Hyun et al. (2020) used consensus clustering on 24-hour BP, heart rate, and sympathetic tone data to derive circadian pattern clusters that were predictive

of 10-year risk of atherosclerotic cardiovascular disease. Additional studies by Paula et al. (2020), Fanelli et al. (2025), and Aristizábal-Ocampo et al. (2025) further demonstrate the application of clustering to ABPM data for clinical phenotyping and risk stratification.

A wide range of clustering methods have been developed, each suited to different data structures. Common approaches include *k*-means clustering, in which a predefined number (*k*) of clusters is selected and observations are assigned iteratively to minimize within-cluster variance, typically using Euclidean distance (McQueen, 1967). Another approach is hierarchical clustering, in which a nested tree-like structure (dendrogram) is constructed by successively merging or splitting clusters based on similarity (Ward Jr., 1963). Additional techniques include density-based methods such as density-based spatial clustering of applications with noise (DBSCAN), which group points based on local density and can identify outliers (Ester et al., 1996); model-based clustering, such as Gaussian Mixture Models (GMMs), which assume data are generated from a mixture of probability distributions (McLachlan & Basford, 1988); spectral clustering, which leverages the eigenvectors of a similarity matrix to reduce dimensionality before clustering (Ng et al., 2001); and self-organizing maps (SOMs), which use neural networks to produce low-dimensional representations of the data (Kohonen, 2002). Algorithms such as *k*-means and GMMs assume fixed-length vector representations and are best suited to static or feature-engineered data. Applying such conventional clustering methods directly to time series is problematic because they ignore the sequential ordering of observations. The temporal structure of ABP data must be taken into account when attempting to create clusters of subjects that exhibit similar dynamic patterns over time.

Additional challenges in clustering time series include irregularly spaced samples, varying series lengths, and missing observations (Alqahtani et al., 2021; Niako et al., 2024; Tan

et al., 2019). A common solution to these challenges is to extract summary features such as the mean, standard deviation, or other statistics, and then apply conventional clustering algorithms to these feature vectors (Ntalianis et al., 2023; Paparrizos et al., 2024a; Wang et al., 2006). Alternatively, some studies have regularized the time axis prior to clustering; for example, Xu et al. (2021) interpolated ABPM readings onto a fixed 15-minute grid and then used Fourier expansions to characterize BP profiles. While these approaches can be effective, they risk discarding temporal information that may be clinically important.

To better preserve temporal structure, specialized time-series similarity measures have been developed that allow to compare sequences directly rather than reducing them to summary features. Dynamic Time Warping (DTW) allows for flexible alignment of time series by "warping" the time axis to account for local phase shifts, making it possible to match similar shapes that are slightly misaligned (Li, H., 2014; Lin et al., 2012; Marteau, 2009; Mueen & Keogh, 2016; Ratanamahatana & Keogh, 2004; Sardá-Espinosa, 2019; Vázquez et al., 2021; Wang et al., 2018; Zakaria et al., 2012; Zhang & Sun, 2023). However, DTW typically requires that series be sampled on the same grid, and it does not inherently resolve differences in length or irregular spacing, so interpolation or preprocessing is often necessary. Time Warp Edit Distance (TWED) extends this idea by incorporating both value differences and timestamp discrepancies, providing a metric distance that can better accommodate uneven sampling (Marteau, 2009).

DTW originated as a technique for measuring similarity between time-dependent sequences and was first widely applied in speech recognition, where it helped align spoken words with reference templates despite variations in speed (Bellman, 1959; Myers, 1980). Instead of measuring the Euclidean distance between each pair of observations at equivalent

indices, DTW allows for local "warping" of the time axis, enabling the comparison of neighboring observations (Figure 2). Sakoe & Chiba (1978) formalized DTW by introducing constraints to improve efficiency and robustness, making it a foundational method for time-series analysis (Berndt & Clifford, 1994; Ratanamahatana & Keogh, 2004).

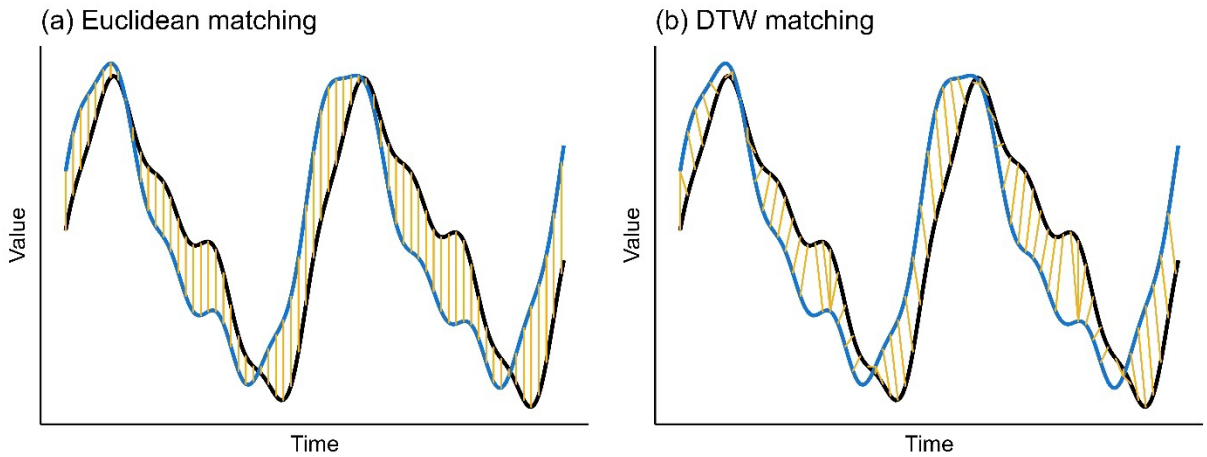

Figure 2: Comparison of Euclidean matching and DTW matching. Yellow lines indicate the distances between matched observations. (a) In Euclidean matching, observations are matched to the same timepoint in the corresponding series. (b) DTW allows observations to be matched with neighboring timepoints in the corresponding series.

DTW has since been widely applied across diverse fields requiring time-series alignment. In bioinformatics, it has been used to compare gene expression profiles, helping to identify similar biological processes across different conditions (Aach & Church, 2001). In finance, DTW has been combined with *k*-medoids clustering to predict stock prices by extracting representative fluctuation patterns from market data (Nakagawa et al., 2019). In neuroscience, DTW has been applied to resting state functional magnetic resonance imaging (fMRI) data, enhancing the identification of distinct brain networks (Philips et al., 2022). More recently, DTW has also been applied directly to BP data: Wang et al. (2018) used DTW to measure similarity between SBP series during hemodialysis sessions in over 14,000 patients with end-stage renal

disease. By combining DTW with a density peak clustering algorithm, they identified five distinct waveform patterns that improved prognostic accuracy for cerebrovascular outcomes compared to conventional BP summary statistics.

TWED, first proposed by Marteau in 2009, builds on the same principle of elastic alignment but introduces a stiffness parameter that penalizes large gaps between aligned points (Marteau, 2009; Paparrizos et al., 2024b). A useful analogy is that of a graphical editor: aligning two series involves either matching points or removing them, with the stiffness parameter controlling how much deviation is permitted. By incorporating both value differences and timestamp discrepancies, TWED provides a structured and interpretable similarity measure particularly well-suited for clinical series with irregular or uneven sampling intervals.

The advantages of TWED have been demonstrated in several medical applications. Liu et al. (2010) used TWED to classify wrist pulse blood flow signals and reported improved classification accuracy over DTW. Jia et al. (2014) embedded TWED within a Gaussian kernel for a support vector machine, achieving substantially lower error in pulse waveform analysis compared to earlier elastic distance methods. Lin et al. (2012) compared multiple elastic distance measures across diverse time-series datasets such as Australian vowel sounds, ECGs, and astronomical star light curves. They found that while DTW remained competitive with a constrained warping window, TWED offered stronger performance when timestamps were irregular.

The application of elastic distance measures such as DTW and TWED to 24-hour ABP data has been limited in prior literature. Accordingly, the objectives of this study are: (1) to compare the DTW and TWED time-series clustering methods in identifying distinct 24-hour

ABP patterns among patients, and (2) to examine the relationships between these BP-derived clusters and patient socio-demographic and clinical characteristics.

CHAPTER II

THEORETICAL BACKGROUND

Clustering and Distance Measures

Cluster analysis refers to the methods that attempt to divide data into subgroups such that the observations within the same group are more similar compared to the observations in different groups. The core concept in any cluster analysis is the notion of similarity and dissimilarity, with degree of dissimilarity commonly based on a distance measure, which is usually defined for a pair of observations. Commonly used distance measures are the L_1 (Manhattan) and L_2 (Euclidean) norms, which quantify similarity or dissimilarity between data points in a vector space (Paparrizos et al., 2024b). The L_1 norm between two points $\mathbf{x} = (x_1, \ldots, x_n)$ and $\mathbf{y} = (y_1, \ldots, y_n)$ is calculated as the sum of the absolute differences of their coordinates:

$$D_{L1}(x, y) = \sum_{i=1}^{n} |x_i - y_i| .$$

In contrast, the L_2 norm measures the straight-line distance between the two points and is given by the square root of the sum of the squared differences:

$$D_{L2}(x, y) = \sqrt{\sum_{i=1}^{n} (x_i - y_i)^2} .$$

The L_1 and L_2 norms are straightforward to compute and constitute true metrics, satisfying properties like non-negativity, symmetry, and the triangle inequality (Lin et al., 2012). However, L_1 and L_2 distances have important limitations when used to cluster multivariate time-series data. They are sensitive to noise, differences in scale, and temporal misalignments, as they

require the series to be of equal length and compare each point in one series directly with its corresponding point in the other. This approach assumes that time points are perfectly aligned; however, if one signal is shifted or lagged, the resulting L_1 or L_2 distance may be large even if the signals are similar in shape. In the context of ABPM data, two patients may have nearly identical circadian patterns, but if one patient's nocturnal dip is delayed by an hour, the Euclidean distance may misleadingly classify them as dissimilar. Additionally, L_2 in particular is sensitive to outliers, and both L_1 and L_2 are affected by differences in scale unless normalization is applied. These limitations motivate the use of elastic distance measures that can accommodate misalignments in time (Aggarwal et al., 2001; Holder et al., 2024; Lemire, 2009; Paparrizos et al., 2024b; Sardá-Espinosa, 2019).

Dynamic Time Warping

The DTW algorithm addresses the alignment issue by allowing nonlinear stretching of the time axis. DTW computes the optimal alignment (warping) between two time series of lengths m and n by constructing a $m \times n$ local cost matrix and finding a minimal-cost path through this matrix. If $\mathbf{x} = (x_1, \ldots, x_m)$ and $\mathbf{y} = (y_1, \ldots, y_n)$ then each cell $D(i, j)$ in the matrix $\mathbf{D}$ contains the distance between x_i and y_j. A warping path $W = ((i_1, j_1), (i_2, j_2), \ldots, (i_k, j_k))$ is a sequence of matrix coordinates that represent an alignment between the points of $\mathbf{x}$ and $\mathbf{y}$. This path must start at the first elements of both series and end at the last elements, i.e. $(i_1,j_1) = (1,1)$ and $(i_K,j_K)=(n,m)$ and it must move monotonically and usually with unit steps (Giorgino, 2009). The DTW distance is defined as the minimum total cost path:

$$\mathrm{D}_{\mathrm{DTW}}(n,m) = \min_{W} \sum_{(i,j)\in W} d(x_i, y_j)$$

subject to predesignated constraints: boundary, monotonicity, continuity, and warping constraints. Under the boundary constraint, the warping path must start at the beginning of both sequences and end at their ends; under the monotonicity constraint, the warping path cannot "go backward in time"; with the continuity (step size) constraint, the path can only move to adjacent cells, ensuring no skipping points; and the warping window constraint prevents excessive stretching.

The optimal warping path can be found by a recursive dynamic programming algorithm that considers the optimal move at each step:

$$\mathrm{D}(i,j) \;=\; |x_i - y_j| + \min\begin{cases} \mathrm{D}(i-1,j) \\ \mathrm{D}(i,j-1) \\ \mathrm{D}(i-1,j-1) \end{cases}$$

with boundary conditions $\mathrm{D}(1,1) = |x_1 - y_1|$.

For multivariate time series, each observation $x_i$and $y_j$is a vector containing multiple variables (e.g., SBP, DBP and MAP). In that case, the local cost at each step is computed using a multivariate L_p norm across variables:

$$\mathrm{lcm}(i,j) = \left(\sum_{v} \left|x_i^{(v)} - y_j^{(v)}\right|^p\right)^{1/p}$$

where v indexes the variables. This ensures that all variables contribute jointly to the distance at each alignment step, allowing DTW to match complete BP profiles rather than treating each variable independently.

As a result, DTW can align points that are shifted in time, effectively warping the sequences to maximize their similarity. For example, an ABPM profile with a delayed BP drop at night could be aligned (warped) to match another profile with an earlier drop, yielding a small DTW distance even if their peaks/troughs do not occur at precisely the same time of day.

The output of DTW includes not only the distance value but also the optimal warping path that minimizes the cumulative cost. This path indicates which points in series **x** correspond to which points in series **y** under the best alignment. Often the path will involve stretches where one index advances while the other stays the same, corresponding to expansion or compression of the time axis. This flexibility allows DTW to overcome limitations of Euclidean distance by finding alignments that minimize shape differences, at the cost of increased computational complexity.

Unconstrained DTW can sometimes produce pathological alignments. For instance, one point in a series may get matched to a large subsection of the other series. To mitigate this, "window" constraints can be applied to limit how far the warping path can stray from the diagonal of the cost matrix. A common constraint is the Sakoe–Chiba band which restricts the warping path to remain within a diagonal corridor of width w, i.e. $|i–j| \leq w$. The effect is that each point in one series can only align with points in the other series that are at most w time steps away in the timeline, preventing excessive time distortion. Typically, a window size around 10% of the series length is used as a rule of thumb, though the optimal window size may depend on the data. Such constraints not only avoid pathological warping (where DTW might overfit by aligning unrelated sections) but can also improve computational efficiency slightly by reducing the matrix area that needs to be explored. It is generally agreed that using no constraint at all is often a poor choice (Mueen & Keogh, 2016).

One drawback of DTW is that it does not satisfy the triangle inequality, which states that for any three points x, y, and z in a metric space, the direct distance between two of the points is never greater than the sum of the two indirect distances:

$$d(x,z) \leq d(x,y) + d(y,z).$$

This means DTW distance is not a true metric, which limits certain applications such as efficient indexing and some hierarchical clustering variants. An additional drawback of DTW is its computational cost. The time and memory complexity of DTW is $O(nm)$, which is quadratic when $n \approx m$. Although DTW can in principle align series of different lengths, linear reinterpolation to a uniform length is generally considered more appropriate; however, restructuring time series to be of equal length and spacing can often be more challenging than the clustering task itself (Ratanamahatana & Keogh, 2004; Zakaria et al., 2012). Since computation times can be prohibitively intensive for long time series or large datasets, numerous pruning and bounding techniques have been developed to speed up DTW-based matching. Perhaps the most common such technique is the *lower bound*, in which an upper and lower envelope are constructed around one time series, as shown in Figure 3. This envelope represents the range of values that would perfectly match the series based on the amount of warping allowed by the window constraint; any candidate series lying completely inside the upper and lower envelope would result in a DTW distance of zero between the two series. By summing the Euclidean distance of observations lying outside the envelope, a guaranteed lower bound on DTW distance can be quickly calculated for any candidate series. If this lower bound already exceeds the best-so-far distance, the full DTW computation can be skipped, which is particularly useful in tasks such as clustering and nearest-neighbor search. The most widely used lower bounds are LB_Keogh and its refinement, LB_Improved (Keogh & Ratanamahatana, 2005; Lemire, 2009; Paparrizos et al., 2024b).

LB_Keogh is defined as

$$LB_{Keogh}(Q, C) = \sqrt{\sum_{i=1}^{n} \begin{cases} (c_i - U_i)^2, if\ c_i > U_i \\ (L_i - c_i)^2, if\ c_i < L_i \\ 0, \quad \text{otherwise} \end{cases}}$$

where C is the contender series, and U_i and L_i are the upper and lower envelopes of the series Q, defined by the window constraint w. If $LB_{Keogh}(Q, C)$ is greater than the current best match, DTW distance calculation for that series can be skipped.

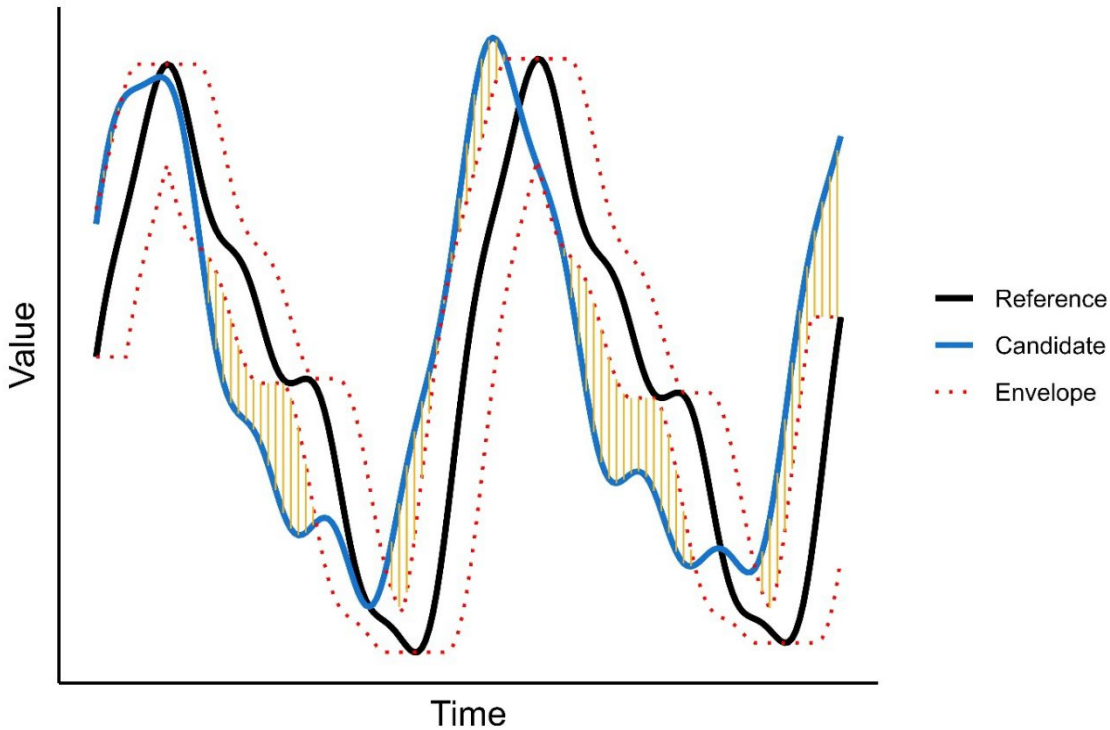

Figure 3: Visualization of the LB_Keogh lower bound for DTW. The envelope surrounding the reference series demarcates the maximum and minimum values that would match each observation in the candidate series with a distance of zero based on the size of the warping window. The yellow lines indicate where observations in the candidate series lie outside the envelope, and the sum of these distances constitutes a lower bound on the total distance between the two series. If this lower bound is greater than the current best match, the full DTW algorithm can be skipped for this candidate.

In time-series clustering, sometimes it may be desirable to represent the average, or centroid, of all time series in a particular cluster. Under Euclidean distance, the centroid is computed by taking the mean of each time point across series. However, under DTW, a straightforward pointwise mean may not be meaningful because points are not aligned one-to-one. DTW Barycenter Averaging (DBA) is an algorithm to compute an average time series that

explicitly accounts for warping alignments. DBA is an iterative heuristic that starts with an initial reference series from the cluster and repeatedly refines it. In each iteration, all series in the cluster are aligned to the current reference using DTW, and at each position of the reference the algorithm computes the average of all series values that were matched to that position. The reference sequence is then updated to these averaged values, producing a new "centroid" sequence. This process continues until convergence. By minimizing the sum of squared DTW distances to the cluster members, DBA produces a centroid that represents the typical shape of the series in that cluster. Petitjean et al. (2011) introduced DBA and demonstrated that it produces more stable and representative prototypes compared to naive averaging or medoid-based approaches.

Time Warp Edit Distance

TWED is an elastic distance measure that, like DTW, allows nonlinear alignments of time series, but it incorporates a notion of edit operations with penalties (Holder et al., 2024; Marteau, 2009). TWED was introduced by Marteau with the goal of combining the strengths of DTW and edit distance (Wagner & Fisher, 1974) while overcoming some of their drawbacks. Unlike DTW, TWED is a true metric: it satisfies the triangle inequality, which ensures that TWED distances can be embedded into metric spaces and used reliably with metric-based algorithms (e.g., *k*-medoids, hierarchical clustering with linkage).

TWED introduces two parameters, a gap penalty λ and stiffness parameter ν. A constant cost of λ is paid for each deletion or insertion of a point in the sequence alignment, and ν controls the penalty for aligning points that are far apart in time. The stiffness parameter effectively places TWED on a spectrum between Euclidean distance and DTW. At one extreme, if the elasticity is extremely low (analogous to setting $\nu = 0$ and a minimal gap penalty), TWED

behaves more like DTW, allowing flexible warping with little penalty on time differences. At the other extreme, with very high stiffness, warping is heavily penalized and TWED approaches the behavior of the Euclidean distance.

Like DTW, TWED is computed via dynamic programming on a cost matrix, but the recursive formulation includes terms for deletion operations and time differences. Suppose we have time series $\mathbf{X} = \{(x_i,t_i)\}$, $i = \{1, \ldots, n\}$ and $\mathbf{Y} = \{(y_j,\tau_j)\}$, $j = \{1, \ldots, m\}$, where t_i and τ_j are the time stamps of the observations. TWED defines a distance $D_{TWED}(i,j)$ as the minimum cost to align the first i points of $\mathbf{X}$ with the first j points of $\mathbf{Y}$. The allowed operations are: *match* (align x_i with y_j), *delete* x_i (align it to a gap), or *delete* y_j. Each operation has an associated cost that includes the Euclidean distance between points being matched (if any), the gap penalty λ for deletions, and a penalty v involving the time difference. The recursive TWED formula can be written as

$$D_{TWED}(i,j) = min\begin{cases} D_{TWED}(i-1,j-1) + \|x_i - y_j\| + \nu|t_i - \tau_j| + \nu|t_{i-1} - \tau_{j-1}|, \\ D_{TWED}(i-1,j) + \|x_i - x_{i-1}\| + \nu|t_i - t_{i-1}| + \lambda, \\ D_{TWED(}(i,j-1) + \|y_j - y_{j-1}\| + \nu|\tau_j - \tau_{j-1}| + \lambda, \end{cases}$$

with $||x_i - y_j||$ being an L_1 or L_2 norm. The time-stamp difference term $|t_i - \tau_j|$ is used in conjunction with ν to penalize matching points that are farther apart in their time index. For deletions, TWED adds the temporal gap between that point and its predecessor in the same series ($|t_i - t_{i-1}|$ or $|\tau_j - \tau_{j-1}|$) to the cost. This ensures that if one series has an extra point that has no counterpart in the other, the cost includes the temporal distance that the extra point spans.

Because of its ability to allow insert and delete operations, an advantage of TWED is that it naturally handles time series of different lengths or with missing data. Additionally, the stiffness parameter also makes TWED well-suited for time-stamped data with irregular intervals, or where time stamps between different series are misaligned. In the context of ABPM, such

cases may occur due to patients starting their monitoring at slightly different times or skipping a reading. Like DTW, the time and memory complexity of TWED is $O(nm)$, but with a larger constant factor due to the additional operations. Marteau's work also introduced a lower bound for TWED, analogous to DTW's lower bounds, to improve computational efficiency. Subsequent research has further explored lower bounds and optimized computation for TWED to make it more tractable for large datasets (Tan et al., 2020).

Partitional Clustering Methods for Time Series

Partitional clustering refers to algorithms that directly partition the dataset into a specified number of clusters, where each time series belongs to one cluster. The two most common partitional methods are *k*-means and *k*-medoids. The *k*-means algorithm seeks to minimize the within-cluster sum of squared distances by iteratively updating cluster assignments and centroids. In the context of time series, a centroid is a prototypical time series that represents the cluster. With conventional Euclidean distance, the centroid is computed by taking the mean of each time coordinate across all series in the cluster. However, if using DTW or TWED as the distance, computing an average is not straightforward because of misalignment. One approach is to use DBA after assigning series to clusters to find the DTW-average series for each cluster, and use those as centroids for the next iteration (Petitjean et al., 2011). DBA *k*-means alternates between (1) assigning series to the closest centroid under DTW and (2) recomputing centroids via DBA, until convergence.

The *k*-medoids method is frequently implemented using the partitioning around medoids (PAM) algorithm (Kaufman & Rousseeuw, 1990), and the two terms are often used interchangeably. In contrast to *k*-means, PAM selects actual observed series as cluster representatives (medoids). This is particularly useful in time-series clustering where synthetic

centroids may not correspond to real physiological patterns. A medoid is an actual data object (in this case, an actual time series from the dataset) that minimizes the sum of distances to other objects in the cluster. PAM works by initializing *k* medoids and then iteratively refining them: it assigns each series to the closest medoid and then tries to swap medoids with non-medoids to improve the clustering. One advantage of PAM for time series is that medoids are guaranteed to be valid time series from the dataset, so they preserve realistic structure. This can be desirable because an average time series (especially under DTW) might produce a smoothed or unnatural sequence that does not actually appear in the data. By using medoids, the cluster center is always a representative series that actually occurred. Many time-series clustering studies opt for PAM because of its simplicity and the well-defined notion of a representative series. The trade-off is that medoids might not be as representative as a true average if the cluster has a lot of variability; the medoid is constrained to be one of the observed series, which might be suboptimal if the true "center" of the cluster lies somewhere between two series. Nonetheless, PAM is often more robust to outliers than *k*-means, since medoids are less influenced by extreme values.

Cluster Validation Indices

After clustering has been performed, cluster validation indices (CVIs) can be used to evaluate the quality of the resulting partitions. CVIs provide quantitative measures of cluster validity by balancing compactness (how similar the objects within each cluster are) and separation (how distinct the clusters are from one another). No single index is universally optimal, so multiple indices are often applied to obtain complementary perspectives. In this study, four CVIs were employed: the Dunn index, silhouette score, a modified Davies–Bouldin index, and the Calinski–Harabasz score.

The Dunn index evaluates the ratio between the minimum inter-cluster distance and the maximum intra-cluster diameter (Paparrizos et al., 2024a; Salgado et al., 2017). Higher values indicate that clusters are well separated relative to their internal spread. A limitation is that the index can be sensitive to noise and outliers, since it depends on extreme distances.

The silhouette score measures the similarity of each observation to its own cluster compared with other clusters (Paparrizos et al., 2024a; Lukasik et al., 2016). For a given point, the silhouette value is defined as

$$s(i) = \frac{b(i) - a(i)}{\max\{a(i), b(i)\}}$$

where *a(i)* is the average distance to other points in the same cluster and *b(i)* is the smallest average distance to points in another cluster. Values close to 1 indicate well-assigned points, values near 0 suggest overlapping clusters, and negative values imply potential misclassification.

The Davies-Bouldin index assesses the average ratio of within-cluster scatter to between-cluster separation, with lower values indicating better clustering (Lukasik et al., 2016; Paparrizos et al., 2024a). In this work, a modified Davies-Bouldin index was used; the modified index incorporates adjustments for time-series data and distance measures beyond Euclidean, improving its applicability to elastic distance measures such as DTW and TWED.

The Calinski-Harabasz score (also known as the Variance Ratio Criterion) measures the ratio of between-cluster dispersion to within-cluster dispersion, scaled by the number of clusters and observations (Lukasik et al., 2016). Higher values indicate better-defined clusters. The index is computationally efficient and often favors partitions with clearly separated and compact clusters.

Sardá-Espinosa (2019) notes that it cannot be determined a priori which CVI will work best, and there is no single best CVI. In addition, CVIs that are commonly used on Euclidean

data may produce different results when applied to time-series clusters. Together, these four indices provide a balanced assessment, capturing different aspects of separation, cohesion, and robustness.

CHAPTER III

METHODS

Study Data

The study data were obtained from the Maracaibo Aging Study which is a prospective, population-based cohort study of individuals aged at least 55 years old residing in Maracaibo, Santa Lucia County, Zulia, Venezuela (Gil et al., 2021; Maestre et al., 2018). Baseline assessment was conducted between 1998 and 2001 whereas follow-up assessments were conducted between 2001 and 2010. The detailed methodology of the study has been described elsewhere (Maestre et al., 2002). The study was approved by the Institutional Review Boards of the Cardiovascular Institute at the University of Zulia in Maracaibo and complied with the Helsinki Declaration for investigations in human participants.

BP readings were obtained at 15 min intervals from 6 a.m. to 11 p.m. and at 30 min intervals from 11 a.m. to 6 a.m. (classified as "night" for all patients) using validated oscillometric 90207 Spacelabs monitors (Snoqualmie, Washington, USA) collecting SBP, DBP, and MAP (Groppelli et al., 1992). All ABPM data were checked and cleaned to avoid errors. Additionally, baseline socio-demographic and clinical variables including age, sex, education level, height, weight, smoking status, presence of diabetes mellitus, serum glucose and cholesterol levels, history of cardiovascular disease or stroke, antihypertensive or antidiabetic medications, as well as cognitive scores (Stein minimental, Folstein minimental, total memory, long-term memory and short-term memory) were recorded.

Data Analysis

A table of descriptive statistics was generated to summarize the baseline characteristics of the study population. Additionally, statistical features including the mean, minimum, maximum, range, SD, COV, ARV, and VIM were generated to describe the overall set of ABP time-series data. These values were calculated for the complete monitoring period as well as separately for nighttime (11:00 pm to 6:00 am) and the remaining daytime. The percentage decrease in mean BP from daytime to nighttime was calculated as the "dipping" statistic (this value was negative where BP increased at night).

Two different clustering algorithms were applied to the time-series data: DTW and TWED. DTW clustering was performed in R using the `dtwclust` package (Sardá-Espinosa, 2019). Data were preprocessed to create equally spaced observations across all series. Because of inconsistencies in the start and end time of each patient's monitoring period, many series did not overlap perfectly. Therefore, a 20-hour window from 12:00 p.m. on day one to 8:00 a.m. on day two was selected to perform the clustering.

DTW clustering was performed using PAM across various parameter combinations, varying the number of clusters (k = 3, 4, and 5) and Sakoe-Chiba window sizes from 1 up to 10. The largest window allowed comparisons up to ten observations apart, corresponding to a difference of 2.5 hours during the day or 5 hours at night. Each series was standardized at the series level prior to clustering to emphasize shape similarities rather than absolute BP levels. Because PAM clustering can be sensitive to the random initialization of medoids, each parameter combination was run three times, for a total of 30 runs. To improve computational efficiency, a maximum of 200 iterations were allowed for convergence.

TWED clustering was performed using the `pytwed` package in Python (Zumer, 2023). The same 20-hour window was used as in the DTW analysis. However, because TWED inherently accommodates misaligned timestamps, no additional time shifting or imputation was performed. TWED parameters were selected following Marteau's original recommendations, with values for the ν parameter of 0.00001, 0.0001, 0.001, 0.01, 0.1, and 1.0, and λ values of 0.0, 0.25, 0.5, 0.75, and 1.0 (Marteau, 2009). Each series was standardized, and TWED distances were calculated separately for SBP, DBP, and MAP; these distances were then combined using the Euclidean norm to yield a single multivariate distance matrix for clustering. From each matrix, clusters of size $k = 3$ and $k = 4$ were generated using PAM clustering.

Clusters were evaluated and characterized using a variety of statistical methods and visual inspection. First, each set of clusters was scored using four different CVIs: Dunn index, silhouette score, a modified Davies-Bouldin index, and Calinski-Harabasz score. Loess-smoothed time-series plots were created for each cluster, showing the standardized mean of SBP, DBP, and MAP as a univariate series. Finally, multidimensional scaling (MDS) was applied to the distance matrices to generate three-dimensional embeddings, with each cluster displayed in a distinct color. Tukey-Kramer multiple comparison tests were used to assess differences between the derived clusters in SBP, DBP, and MAP descriptive statistics. Significant findings were visualized using radar charts. Patient hypertension was classified using the American Heart Association (AHA) 2017 guidelines (Table 1).

Table 1: AHA hypertension thresholds.

Ambulatory Hypertension Measure	24-hour BP	Daytime BP	Nighttime BP
SBP (mmHg) / DBP (mmHg)	≥ 125 / ≥ 75	≥ 130 / ≥ 80	≥ 110 / ≥ 65
MAP (mmHg)	≥ 92	≥ 96	≥ 82

Abbreviations: BP, blood pressure; DBP, diastolic blood pressure; MAP, mean arterial pressure; SBP, systolic blood pressure.

Baseline patient characteristics and cognitive scores were compared between clusters using one-way ANOVA for numerical variables, and either chi-squared or Fisher exact test as appropriate for categorical variables. Pairwise post-hoc tests were performed using Tukey-Kramer multiple comparison tests for numerical variables and a pairwise chi-squared test for categorical variables. Finally, DTW and TWED clusters were cross-tabulated and tested for independence using Pearson's chi-squared test. All statistical tests were two-sided and were based on a significance level of 0.05. Statistical analysis was performed using R 4.4.0 (R Foundation for Statistical Computing, Vienna, Austria) and SAS 9.4 (SAS Institute Inc., Cary, NC, USA).

CHAPTER IV

RESULTS

Descriptive Statistics

A total of 2,155 BP time series were used for the clustering. Baseline analysis was applied to the 736 distinct patients who had 24-hour ABP recorded on the same date as their baseline clinical data was collected. Descriptive characteristics of the baseline population are shown in Table 2. The mean patient age was 64.9 years (SD 7.5) and 274 (37.8%) were male. The mean BMI of the patients was 27.4 kg/m^2 (SD 4.9). Around half of the patients (n = 363; 50.8%) were smokers, and 182 (25.2%) were alcohol drinkers. Diabetes mellitus was present in 142 of the patients (19.7%) and 94 (13.0%) had a history of cardiovascular disease.

As shown in Table 3, all three BP measures (SBP, DBP, and MAP) had positive mean dipping (i.e. they decreased at night). DBP dipped by the most (mean = 7.3, SD = 8.3) while SBP dipped the least (mean = 3.9, SD = 7.1). In terms of variability, when compared to DBP, SBP had a higher mean SD, ARV, and VIM, whereas DBP had higher COV, on average.

Table 2: Summary of patient baseline socio-demographic and clinical characteristics (n=736).

Categorical variables	***n* (%)**
Male	274 (37.8)
Dyslipidemia	170 (23.6)
Smoker	363 (50.8)
Alcohol drinker	182 (25.2)
Diabetes mellitus	142 (19.7)
Treated hypertension	205 (28.4)
Cardiovascular disease	94 (13.0)
Continuous variables	**mean (SD)**
Age (years)	64.9 (7.5)
Education (years)	6.7 (4.1)
Weight (kg)	68.3 (13.6)
Height (m)	1.58 (0.09)
BMI (kg/m^2)	27.4 (4.9)
Serum glucose (mg/dL)	112.6 (51.6)
Total cholesterol (mg/dL)	190.6 (59.7)
Triglycerides (mg/dL)	162.7 (109.8)

Abbreviations: BMI, body mass index; SD, standard deviation.

Table 3: Summary of ambulatory blood pressure statistics.

Variable	**SBP (mmHg) mean (SD)**	**DBP (mmHg) mean (SD)**	**MAP (mmHg) mean (SD)**
Dipping	3.9 (7.1)	7.3 (8.3)	5.2 (7.5)
Maximum	159.7 (22.8)	97.6 (12.9)	119.9 (15.6)
Mean	127.0 (16.1)	72.5 (9.4)	92.1 (11.0)
Minimum	101.2 (14.6)	52.1 (8.9)	69.6 (10.5)
Range	58.5 (16.8)	45.6 (10.9)	50.3 (12.5)
SD	12.4 (3.3)	9.8 (2.2)	10.7 (2.5)
COV	9.8 (2.4)	13.7 (3.1)	11.7 (2.5)
ARV	9.2 (1.9)	7.8 (1.6)	8.4 (1.7)
VIM	12.4 (3.0)	9.9 (2.1)	10.7 (2.3)

Abbreviations: ARV, average real variability; COV, coefficient of variation; DBP, diastolic blood pressure; MAP, mean arterial pressure; SBP, systolic blood pressure; SD, standard deviation; VIM, variability independent of the mean.

DTW-Derived Clusters

Based on the CVIs and visual inspection of the time-series patterns (Table 4, Figures 6 & 7), the final DTW model selected had three clusters using a Sakoe–Chiba window size of 1 (meaning it looked for the best match either at the same observation, or one observation either side). This configuration produced a silhouette score of 0.046, Dunn index of 0.297, Modified Davies–Bouldin index of 1.957, and Calinski–Harabasz score of 954.10. The three clusters contained 349, 865, and 933 time series, respectively.

Cluster 1 was associated with negative nighttime dipping (higher BP at night than during the day) along with high nighttime minimum, maximum, and mean BP (Table 4, Figures 4, 5 & 8). Cluster 1 also had low COV for DBP and MAP, both at night and across the entire recording period. Cluster 3, conversely, had significantly higher levels of dipping and lower nighttime minimum, maximum, and mean BP compared to the other clusters. Cluster 3 also exhibited high levels of SD, COV, and VIM both at nighttime and over the whole recording period, although some daytime variability measures were lower. Cluster 2 was often significantly higher than one of the other clusters and/or significantly lower than the other, generally being ranked between the other two clusters on many measures.

Cluster 1 had the highest incidence of ABP hypertension, particularly at night, with 320 patients (91.7%) above the nocturnal hypertension threshold for SBP, 281 (80.5%) for DBP, and 301 (86.2%) for MAP. The cluster with the lowest observed nocturnal hypertension was Cluster 3; nonetheless, even in this cluster as many as 64.1% of participants recorded nocturnal SBP hypertension, along with 51.3% for MAP and 46.0% for DBP. The distribution of nighttime mean BP can be seen in Figure 4. Daytime hypertension incidence was broadly similar among the three clusters.

Table 4: Comparison of ABP descriptive statistics across DTW-derived clusters.

Descriptive statistic	**Cluster 1^ (*n* = 349)**	**Cluster 2^ (*n* = 865)**	**Cluster 3^ (*n* = 933)**	**Cluster 1 vs. Cluster 2**	**Cluster 1 vs. Cluster 3**	**Cluster 2 vs. Cluster 3**
Continuous variable	mean (SE)	mean (SE)	mean (SE)	Tukey-Kramer p-value	Tukey-Kramer p-value	Tukey-Kramer p-value
Dipping DBP	-1.4 (0.32)	4.4 (0.20)	13.3 (0.20)	< 0.001	< 0.001	< 0.001
Dipping MAP	-3.2 (0.28)	2.6 (0.18)	10.9 (0.17)	< 0.001	< 0.001	< 0.001
Dipping SBP	-4.2 (0.27)	1.7 (0.17)	9.0 (0.17)	< 0.001	< 0.001	< 0.001
Maximum DBP	98.9 (0.67)	98.0 (0.43)	96.9 (0.41)	0.518	0.031	0.142
Maximum DBP (Day)	97.8 (0.67)	97.5 (0.43)	96.6 (0.41)	0.929	0.280	0.276
Maximum DBP (Night)	88.3 (0.66)	84.2 (0.42)	79.5 (0.41)	< 0.001	< 0.001	< 0.001
Maximum MAP	120.6 (0.82)	121.0 (0.52)	118.8 (0.50)	0.896	0.155	0.007
Maximum MAP (Day)	119.3 (0.81)	120.3 (0.52)	118.6 (0.50)	0.568	0.698	0.040
Maximum MAP (Night)	111.5 (0.77)	106.1 (0.49)	99.0 (0.47)	< 0.001	< 0.001	< 0.001
Maximum SBP	161.7 (1.19)	161.6 (0.76)	157.3 (0.73)	0.994	0.005	< 0.001
Maximum SBP (Day)	159.1 (1.18)	160.6 (0.75)	157.0 (0.72)	0.507	0.305	0.002
Maximum SBP (Night)	152.2 (1.08)	144.0 (0.69)	134.3 (0.67)	< 0.001	< 0.001	< 0.001
Mean DBP	73.6 (0.50)	72.5 (0.31)	72.2 (0.30)	0.155	0.057	0.837
Mean DBP (Day)	73.4 (0.50)	73.2 (0.32)	74.5 (0.31)	0.966	0.127	0.010
Mean DBP (Night)	74.3 (0.52)	70.0 (0.33)	64.6 (0.32)	< 0.001	< 0.001	< 0.001
Mean MAP	94.1 (0.57)	92.3 (0.37)	91.2 (0.35)	0.028	< 0.001	0.078
Mean MAP (Day)	93.4 (0.58)	92.8 (0.37)	93.5 (0.36)	0.689	0.976	0.351
Mean MAP (Night)	96.3 (0.60)	90.5 (0.38)	83.3 (0.37)	< 0.001	< 0.001	< 0.001
Mean SBP	130.1 (0.84)	127.6 (0.54)	125.4 (0.52)	0.035	< 0.001	0.009
Mean SBP (Day)	128.9 (0.85)	128.1 (0.54)	128.0 (0.52)	0.701	0.678	0.999
Mean SBP (Night)	134.1 (0.88)	125.9 (0.56)	116.5 (0.54)	< 0.001	< 0.001	< 0.001
Minimum DBP	54.1 (0.46)	52.8 (0.29)	50.7 (0.28)	0.051	< 0.001	< 0.001
Minimum DBP (Day)	54.9 (0.49)	54.1 (0.31)	54.8 (0.30)	0.353	0.978	0.255

Table 4 cont.

Minimum DBP (Night)	61.7 (0.51)	57.7 (0.33)	52.4 (0.32)	< 0.001	< 0.001	< 0.001
Minimum MAP	71.4 (0.54)	70.7 (0.35)	68.0 (0.33)	0.533	< 0.001	< 0.001
Minimum MAP (Day)	72.0 (0.56)	71.8 (0.36)	72.0 (0.35)	0.959	1.000	0.917
Minimum MAP (Night)	82.3 (0.59)	77.3 (0.38)	70.4 (0.36)	< 0.001	< 0.001	< 0.001
Minimum SBP	102.9 (0.76)	102.9 (0.48)	99.1 (0.47)	0.999	< 0.001	< 0.001
Minimum SBP (Day)	103.7 (0.77)	104.2 (0.49)	104.1 (0.47)	0.822	0.898	0.975
Minimum SBP (Night)	117.2 (0.84)	110.3 (0.54)	101.4 (0.52)	< 0.001	< 0.001	< 0.001
Range DBP	44.8 (0.58)	45.2 (0.37)	46.2 (0.35)	0.825	0.106	0.139
Range DBP (Day)	42.9 (0.57)	43.4 (0.36)	41.8 (0.35)	0.731	0.242	0.005
Range DBP (Night)	26.6 (0.52)	26.5 (0.33)	27.1 (0.32)	0.963	0.771	0.416
Range MAP	49.1 (0.66)	50.3 (0.42)	50.8 (0.41)	0.326	0.082	0.624
Range MAP (Day)	47.4 (0.66)	48.5 (0.42)	46.6 (0.40)	0.298	0.569	0.003
Range MAP (Night)	29.2 (0.55)	28.8 (0.35)	28.6 (0.34)	0.807	0.636	0.929
Range SBP	58.8 (0.89)	58.6 (0.56)	58.3 (0.54)	0.994	0.885	0.879
Range SBP (Day)	55.4 (0.88)	56.4 (0.56)	53.0 (0.54)	0.601	0.049	< 0.001
Range SBP (Night)	35.0 (0.64)	33.8 (0.41)	32.9 (0.39)	0.237	0.015	0.280
SD DBP	9.5 (0.12)	9.7 (0.07)	10.1 (0.07)	0.140	< 0.001	< 0.001
SD DBP (Day)	9.6 (0.12)	9.9 (0.08)	9.3 (0.07)	0.120	0.123	< 0.001
SD DBP (Night)	7.8 (0.15)	7.8 (0.09)	8.0 (0.09)	0.927	0.581	0.165
SD MAP	10.4 (0.13)	10.6 (0.08)	10.9 (0.08)	0.400	0.002	0.018
SD MAP (Day)	10.5 (0.14)	10.9 (0.09)	10.3 (0.08)	0.087	0.203	< 0.001
SD MAP (Night)	8.5 (0.15)	8.5 (0.10)	8.4 (0.09)	0.960	0.917	0.985
SD SBP	12.5 (0.17)	12.3 (0.11)	12.4 (0.11)	0.730	0.943	0.831
SD SBP (Day)	12.3 (0.18)	12.6 (0.12)	11.6 (0.11)	0.568	0.003	< 0.001
SD SBP (Night)	10.3 (0.18)	10.0 (0.12)	9.6 (0.11)	0.389	0.007	0.060
COV DBP	13.0 (0.16)	13.5 (0.10)	14.1 (0.10)	0.006	< 0.001	< 0.001
COV DBP (Day)	13.2 (0.17)	13.6 (0.11)	12.6 (0.10)	0.077	0.011	< 0.001
COV DBP (Night)	10.6 (0.21)	11.2 (0.14)	12.5 (0.13)	0.046	< 0.001	< 0.001
COV MAP	11.1 (0.13)	11.6 (0.08)	12.0 (0.08)	0.010	< 0.001	< 0.001

Table 4 cont.

COV MAP (Day)	11.3 (0.14)	11.8 (0.09)	11.0 (0.08)	0.013	0.146	< 0.001
COV MAP (Night)	8.9 (0.17)	9.4 (0.11)	10.1 (0.10)	0.022	< 0.001	< 0.001
COV SBP	9.6 (0.12)	9.7 (0.08)	9.9 (0.08)	0.823	0.096	0.124
COV SBP (Day)	9.6 (0.13)	9.8 (0.08)	9.1 (0.08)	0.248	0.002	< 0.001
COV SBP (Night)	7.7 (0.14)	8.0 (0.09)	8.3 (0.09)	0.143	0.001	0.049
ARV DBP	7.9 (0.08)	7.7 (0.05)	7.9 (0.05)	0.242	0.941	0.199
ARV DBP (Day)	6.2 (0.07)	6.1 (0.05)	6.0 (0.04)	0.672	0.320	0.720
ARV DBP (Night)	2.0 (0.04)	1.9 (0.02)	1.9 (0.02)	0.863	0.764	0.970
ARV MAP	8.5 (0.09)	8.4 (0.06)	8.5 (0.06)	0.308	0.718	0.617
ARV MAP (Day)	6.7 (0.08)	6.6 (0.05)	6.6 (0.05)	0.442	0.219	0.834
ARV MAP (Night)	2.1 (0.04)	2.1 (0.03)	2.0 (0.02)	0.801	0.407	0.029
ARV SBP	9.4 (0.10)	9.2 (0.06)	9.2 (0.06)	0.144	0.051	0.833
ARV SBP (Day)	7.3 (0.08)	7.2 (0.05)	7.0 (0.05)	0.264	0.013	0.218
ARV SBP (Night)	2.4 (0.05)	2.5 (0.03)	2.3 (0.03)	0.836	0.007	< 0.001
VIM DBP	9.4 (0.11)	9.7 (0.07)	10.2 (0.07)	0.029	< 0.001	< 0.001
VIM DBP (Day)	9.6 (0.12)	9.9 (0.08)	9.3 (0.07)	0.082	0.042	< 0.001
VIM DBP (Night)	7.5 (0.14)	7.7 (0.09)	8.2 (0.09)	0.618	< 0.001	< 0.001
VIM MAP	10.3 (0.12)	10.6 (0.08)	11.0 (0.07)	0.036	< 0.001	0.001
VIM MAP (Day)	10.5 (0.13)	10.9 (0.08)	10.3 (0.08)	0.019	0.153	< 0.001
VIM MAP (Night)	8.1 (0.15)	8.3 (0.09)	8.7 (0.09)	0.262	< 0.001	0.009
VIM SBP	12.2 (0.16)	12.3 (0.10)	12.6 (0.10)	0.900	0.165	0.163
VIM SBP (Day)	12.3 (0.17)	12.6 (0.10)	11.6 (0.10)	0.260	0.002	< 0.001
VIM SBP (Night)	9.6 (0.17)	9.8 (0.11)	10.1 (0.11)	0.382	0.036	0.289
Categorical variable	n (%)	n (%)	n (%)	χ^2 p-value	χ^2 p-value	χ^2 p-value
Hypertensive SBP	198 (56.7)	445 (51.4)	432 (46.3)	0.095	0.002	0.059
Hypertensive SBP (Day)	148 (42.4)	348 (40.2)	386 (41.4)	1.000	1.000	1.000
Hypertensive SBP (Night)	320 (91.7)	711 (82.2)	598 (64.1)	< 0.001	< 0.001	< 0.001
Hypertensive DBP	148 (42.4)	307 (35.5)	315 (33.8)	0.048	0.012	0.441
Hypertensive DBP (Day)	84 (24.1)	192 (22.2)	242 (25.9)	0.962	0.962	0.192

Table 4 cont.

Hypertensive DBP (Night)	281 (80.5)	589 (68.1)	429 (46.0)	< 0.001	< 0.001	< 0.001
Hypertensive MAP	192 (55.0)	401 (46.4)	401 (43.0)	0.013	< 0.001	0.150
Hypertensive MAP (Day)	130 (37.2)	286 (33.1)	354 (37.9)	0.328	0.820	0.093
Hypertensive MAP (Night)	301 (86.2)	644 (74.5)	479 (51.3)	< 0.001	< 0.001	< 0.001
Dipping SBP				< 0.001	< 0.001	< 0.001
Reverse (≤ 0)	256 (73.4)	293 (33.9)	18 (1.9)			
Non- (> 0 to ≤ 10)	91 (26.1)	536 (62.0)	562 (60.2)			
Normal (> 10 to ≤ 20)	2 (0.6)	36 (4.2)	338 (36.2)			
Extreme (> 20)	0 (0.0)	0 (0.0)	15 (1.6)			
Dipping DBP				< 0.001	< 0.001	< 0.001
Reverse (≤ 0)	194 (55.6)	198 (22.9)	6 (0.6)			
Non- (> 0 to ≤ 10)	147 (42.1)	506 (58.5)	279 (29.9)			
Normal (> 10 to ≤ 20)	8 (2.3)	160 (18.5)	520 (55.7)			
Extreme (> 20)	0 (0.0)	1 (0.1)	128 (13.7)			
Dipping MAP				< 0.001	< 0.001	< 0.001
Reverse (≤ 0)	241 (69.1)	256 (29.6)	3 (0.3)			
Non- (> 0 to ≤ 10)	107 (30.7)	549 (63.5)	432 (46.3)			
Normal (> 10 to ≤ 20)	1 (0.3)	60 (6.9)	452 (48.4)			
Extreme (> 20)	0 (0.0)	0 (0.0)	46 (4.9)			

Abbreviations: ARV, average real variability; COV, coefficient of variation; DBP, diastolic blood pressure; MAP, mean arterial pressure; SBP, systolic blood pressure; SD, standard deviation; SE, standard error; VIM, variability independent of the mean.
^Green fill denotes cluster with highest value where significantly different from the other two clusters. Red fill denotes cluster with lowest value where significantly different from the other two clusters.

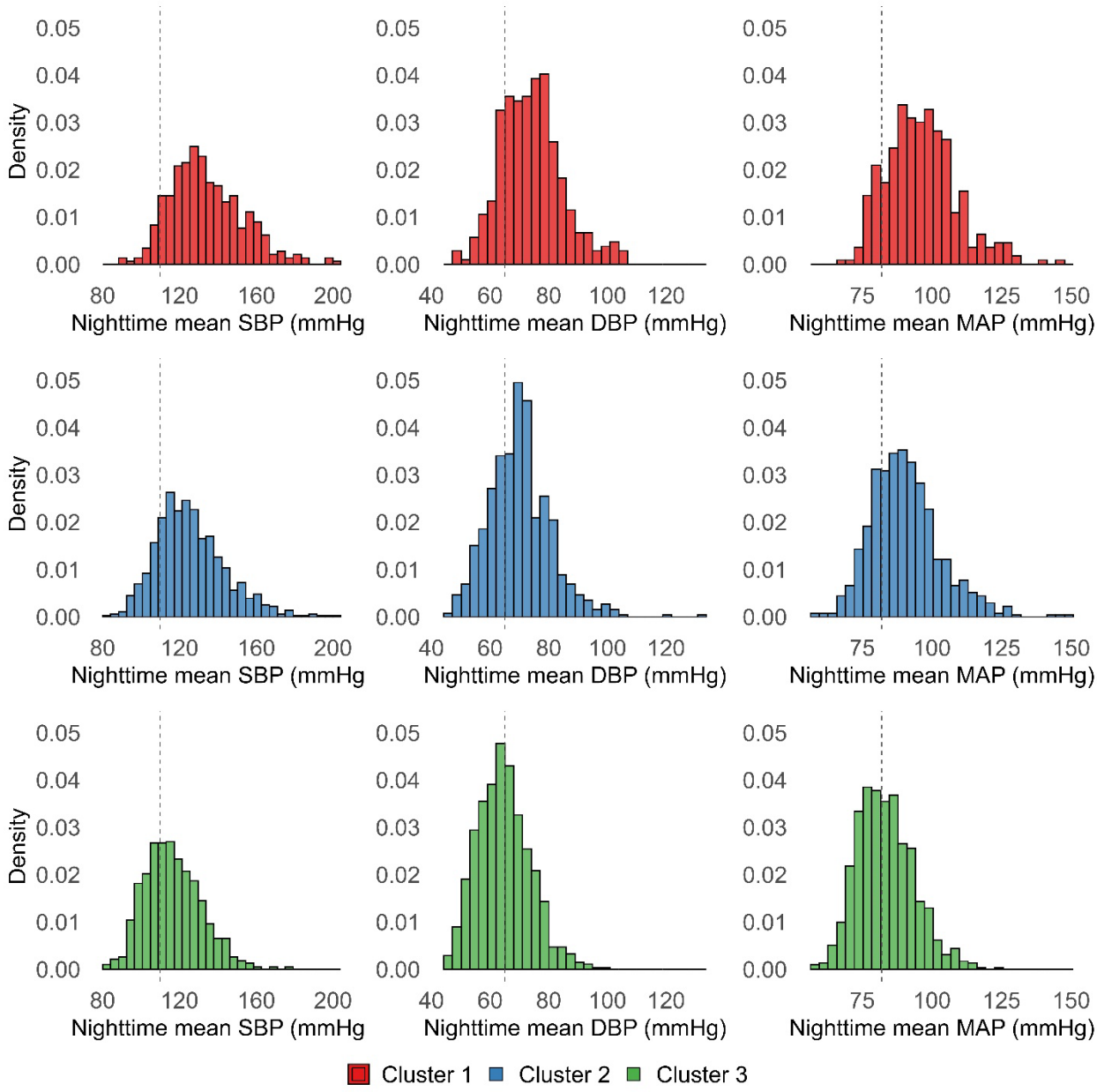

Figure 4: Histograms of nighttime mean DBP, MAP and SBP for DTW-derived clusters. Dotted lines denote respective hypertension thresholds. Abbreviations: DBP, diastolic blood pressure; DTW, dynamic time warping; MAP, mean arterial pressure; SBP, systolic blood pressure.

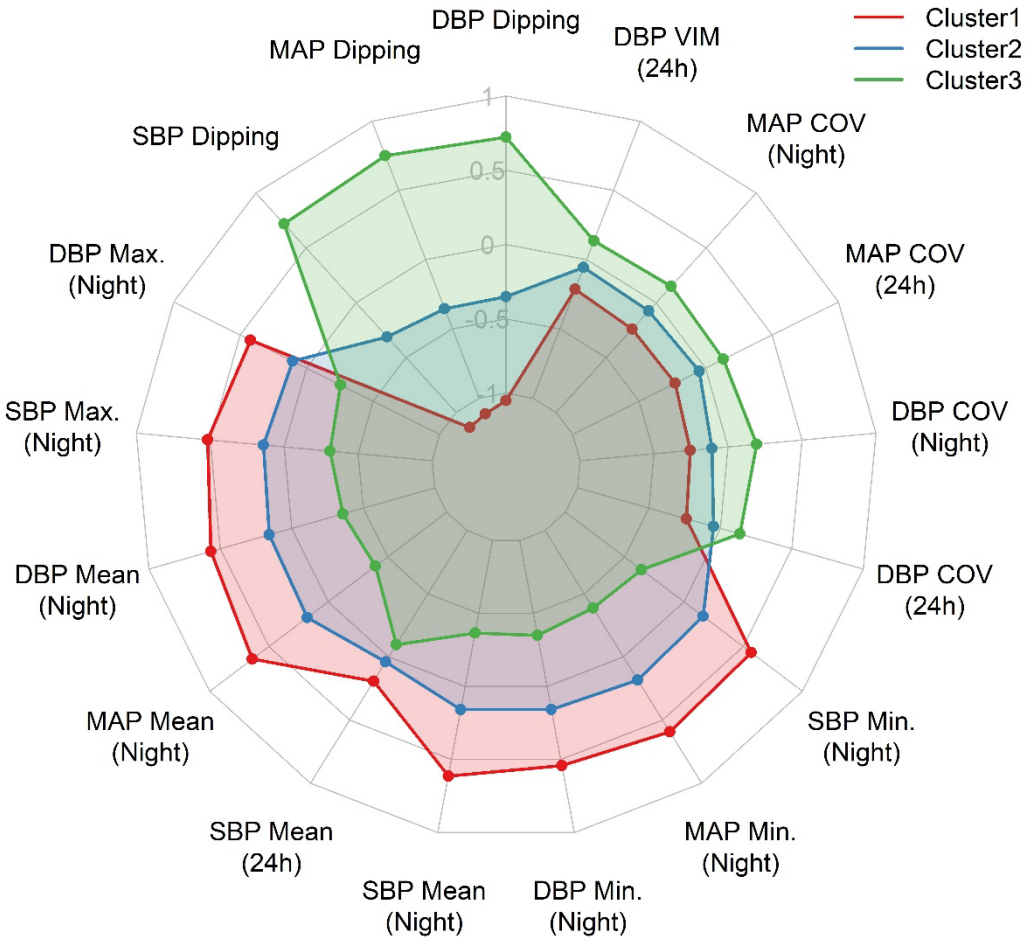

Figure 5: Radar chart showing standardized values for significantly different continuous ABP variables across DTW-derived clusters. Abbreviations: ABP, ambulatory blood pressure; COV, coefficient of variation; DBP, diastolic blood pressure; DTW, dynamic time warping; MAP, mean arterial pressure; SBP, systolic blood pressure; VIM, variability independent of the mean.

The overall shapes of the mean BP trajectories across the monitoring period for the three clusters are shown in Figure 6. Cluster 1 can be seen dipping in the afternoon around 14:00 then steadily rising until 20:00, and then after a short dip rising again from 22:00 throughout the night. Cluster 3 displays a distinct nighttime dip, reaching almost one standard deviation below the standardized mean BP around 02:00 in the morning. Cluster 2 exhibits the same double dip shape as Cluster 3 but with nowhere near the same nighttime drop in BP. The multidimensional

scaling plot in Figure 7 reiterates the distinct separation between Clusters 1 and 3, with Cluster 2 in between.

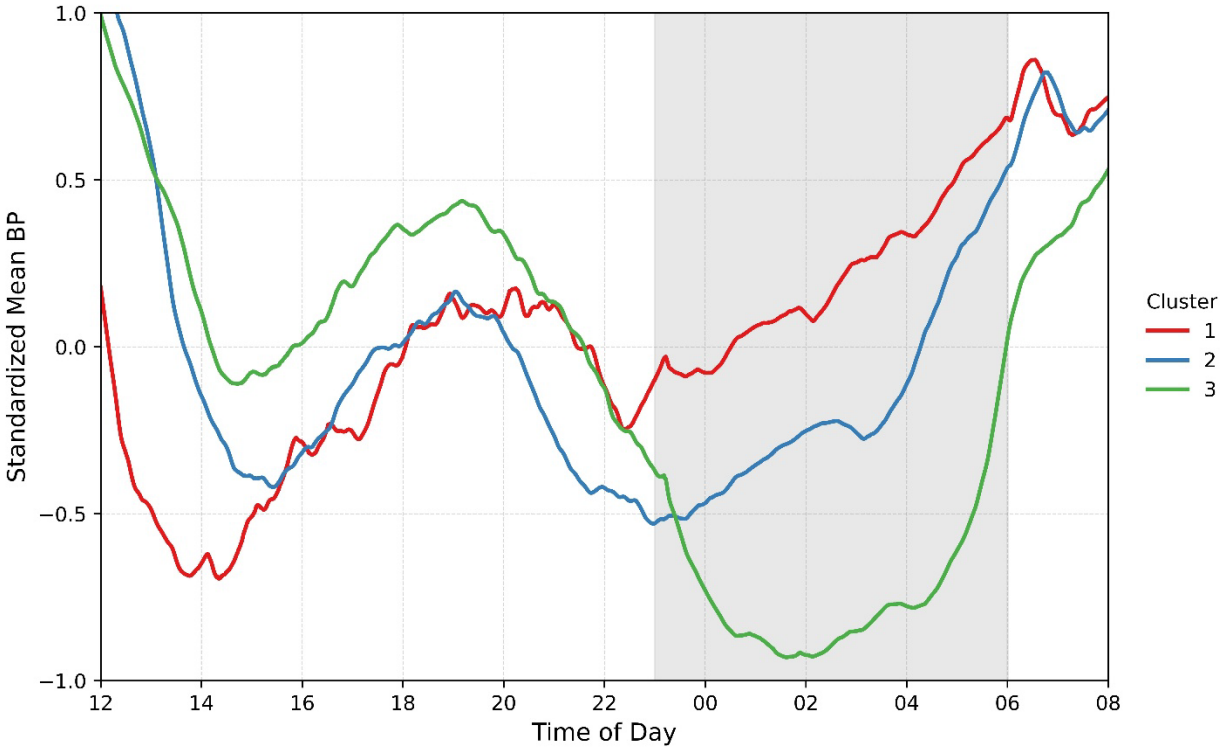

Figure 6: Loess-smoothed series means for DTW-derived clusters. The line for each cluster represents the mean of the standardized values for SBP, DBP and MAP at each timepoint. Designated nighttime hours are marked with gray background. Abbreviations: BP, blood pressure; DBP, diastolic blood pressure; DTW, dynamic time warping; MAP, mean arterial pressure; SBP, systolic blood pressure.

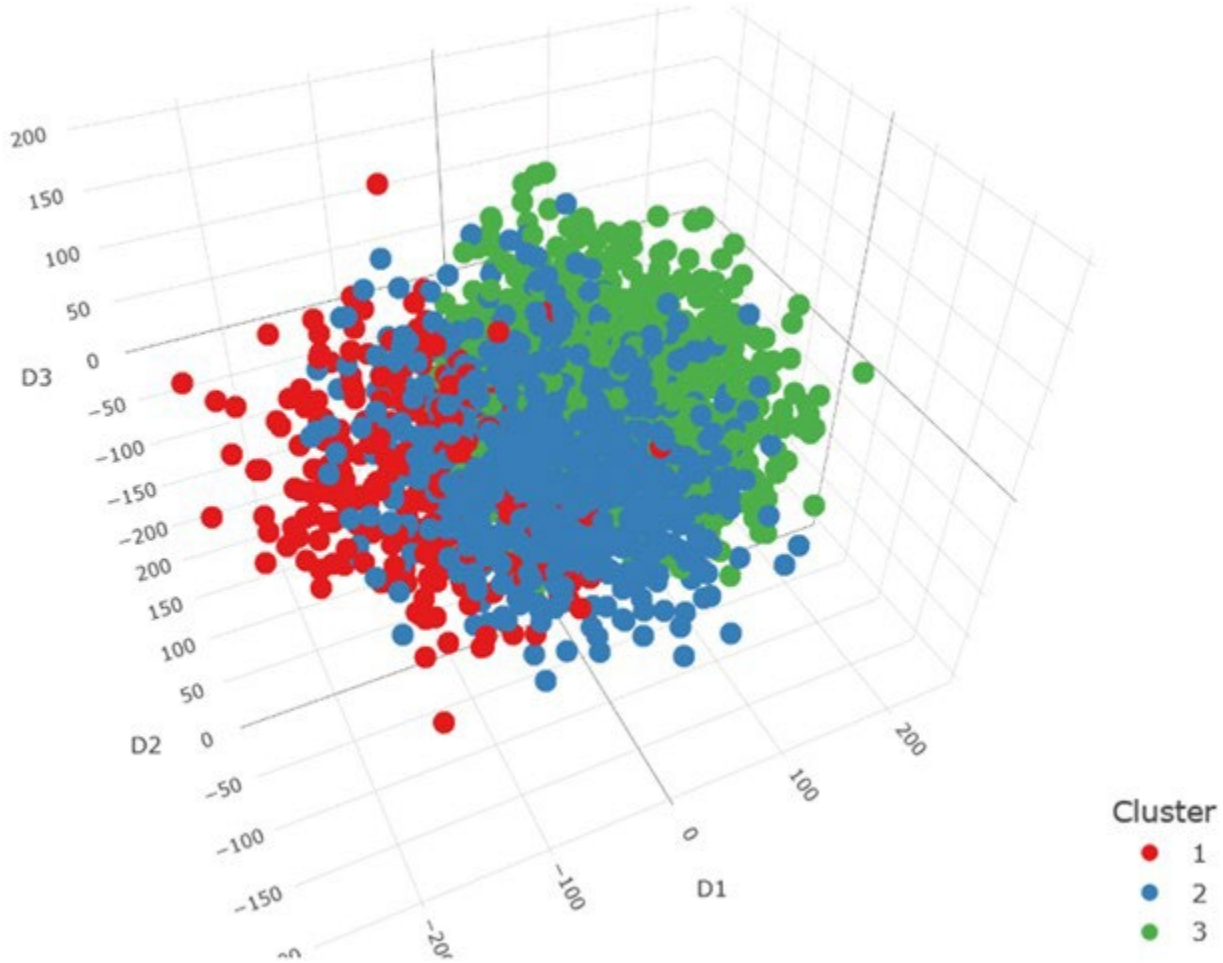

Figure 7: Multidimensional scaling (3D) representation of DTW-derived clusters.

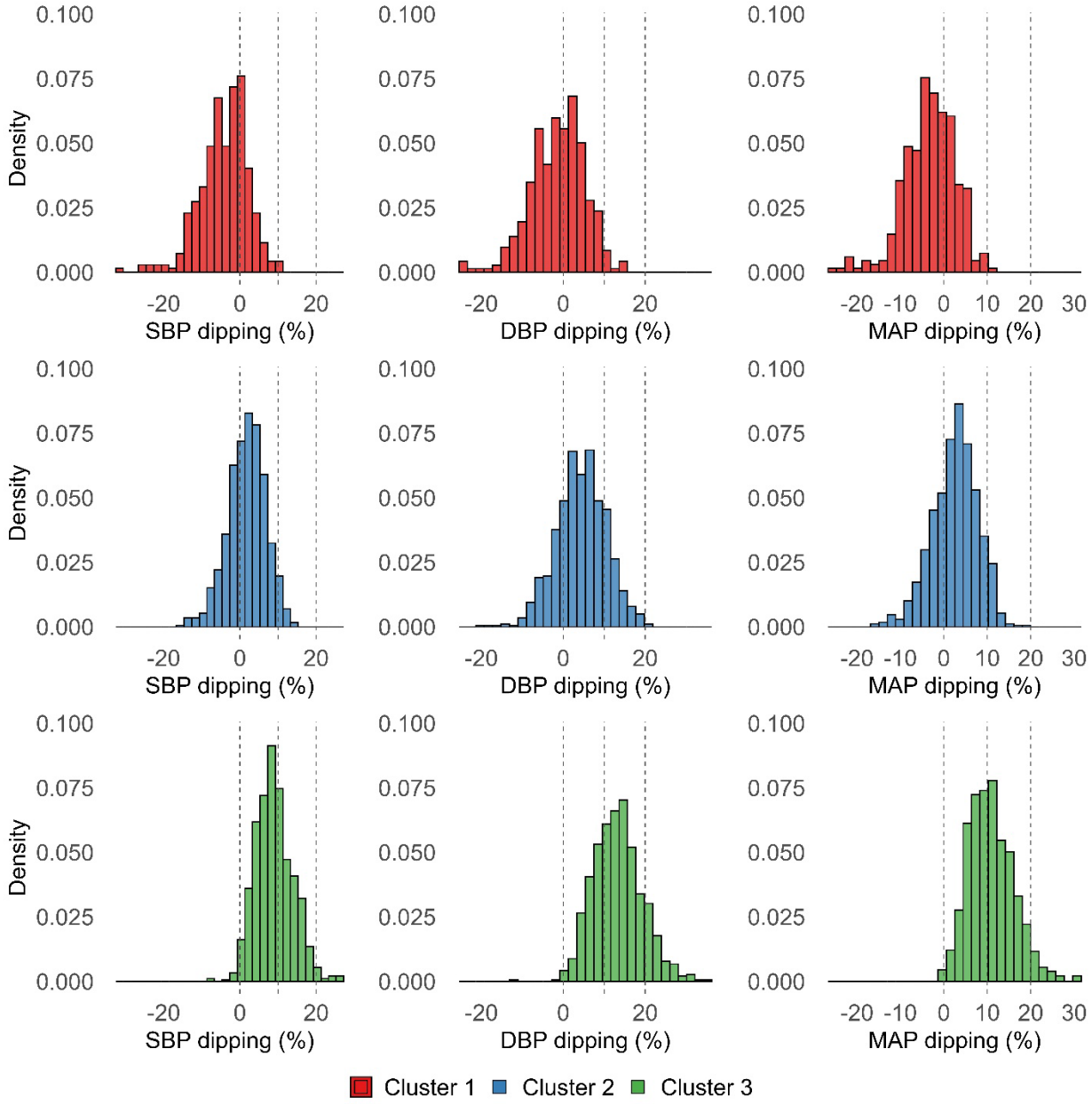

Figure 8: Histograms of DBP, MAP and SBP dipping % for DTW-derived clusters. Dotted lines denote dipping thresholds. Reverse dipping < 0; non-dipping ≥ 0 to < 10; normal dipping ≥ 10 to < 20; extreme dipping ≥ 20. Abbreviations: DBP, diastolic blood pressure; DTW, dynamic time warping; MAP, mean arterial pressure; SBP, systolic blood pressure.

Table 5: Characterization of DTW-derived clusters.

Cluster	Characterization	Pattern Summary	Clinical Interpretation
1	"Non-dippers"	Minimal or negative nighttime dipping with highest nighttime hypertension, low 24h and nighttime COV.	Reverse dipping and nocturnal hypertension pattern; associated with higher cardiovascular and cognitive risk.
2	"Moderate dippers"	Moderate nighttime BP decline and nocturnal hypertension with midrange variability measures over 24 hours.	Transitional dipping profile with nighttime hypertension and intermediate risk.
3	"Strong dippers"	Clear nighttime BP reduction (10–20%), low daytime variability, high nighttime and 24h variability but lower night ARV.	Physiologic dipping pattern with lower cardiovascular and cognitive risk.

Abbreviations: ARV, average real variability; BP, blood pressure; COV, coefficient of variation.

In the comparison of baseline characteristics between DTW clusters (Table 6), age, education, triglycerides and treated hypertension were found to have a significant overall difference among the clusters. The highest mean age was in the moderate dippers (66.18 years; SD 7.74) and the lowest was in the strong dippers (63.75 years; SD 7.06). The pairwise difference between these two clusters was statistically significant ($p < 0.001$). Conversely, the strong dippers had the highest mean number of years of education (7.15 years; SD 4.42) and the moderate dippers had the lowest (6.27 years; SD 3.74), also with a significant pairwise difference ($p = 0.017$).

Patients in the non-dipping cluster had the highest level of triglycerides (195.84 mg/dL; SD 164.48) and the moderate dippers had the lowest (149.11 mg/dL; SD 90.03) with a significant pairwise difference ($p = 0.039$). The moderate dippers had the highest proportion of patients with treated hypertension ($n = 112$; 35.3%). This was significantly higher than both the non-dippers and the strong dippers ($p = 0.009$ and $p = 0.001$, respectively) in the pairwise

analysis. Finally, the non-dippers recorded the highest mean score in all five cognitive tests. However, the one-way ANOVA test was not statistically significant for any of the five scores.

Table 6: Comparison of baseline socio-demographic and clinical characteristics between DTW-derived clusters.

Characteristic	**Cluster 1 (Non-dippers) (n=77)**	**Cluster 2 (Moderate dippers) (n=322)**	**Cluster 3 (Strong dippers) (n=337)**	**Overall p-value**	**Cluster 1 vs. Cluster 2**	**Cluster 1 vs. Cluster 3**	**Cluster 2 vs. Cluster 3**
Continuous variable	mean (SD)	mean (SD)	mean (SD)	ANOVA F-test p-value	Tukey-Kramer p-value	Tukey-Kramer p-value	Tukey-Kramer p-value
Age (years)	64.47 (7.01)	66.18 (7.74)	63.75 (7.06)	<0.001	0.161	0.713	< 0.001
Education (years)	6.66 (4.10)	6.27 (3.74)	7.15 (4.42)	0.024	0.736	0.603	0.017
Weight (kg)	69.19 (13.50)	68.21 (13.16)	68.18 (14.01)	0.833	0.836	0.824	0.999
Height (m)	1.57 (0.09)	1.57 (0.09)	1.58 (0.09)	0.313	0.873	0.418	0.436
BMI (kg/m^2)	28.13 (5.23)	27.46 (4.63)	27.17 (4.97)	0.281	0.520	0.255	0.711
Serum glucose (mg/dL)	127.26 (56.50)	108.68 (48.41)	113.71 (53.35)	0.110	0.094	0.278	0.573
Total cholesterol (mg/dL)	181.15 (62.36)	191.82 (63.73)	191.26 (55.20)	0.582	0.554	0.587	0.995
Triglycerides (mg/dL)	195.84 (164.48)	149.11 (90.03)	169.66 (113.45)	0.024	0.039	0.352	0.130
Stein minimental	45.79 (6.76)	44.19 (7.27)	44.90 (7.63)	0.184	0.201	0.602	0.436
Folstein minimental	24.71 (3.49)	23.91 (3.93)	24.43 (3.98)	0.126	0.237	0.836	0.202
Total memory	38.87 (8.69)	38.32 (9.04)	38.28 (9.62)	0.877	0.885	0.867	0.998
Short term memory	5.62 (2.13)	5.43 (2.19)	5.43 (2.27)	0.781	0.771	0.784	0.999
Long term memory	25.16 (11.78)	24.71 (11.27)	24.51 (12.26)	0.909	0.951	0.901	0.975
Categorical variable	n (%)	n (%)	n (%)	Overall χ^2 test p-value	Pairwise χ^2 test p-value	Pairwise χ^2 test p-value	Pairwise χ^2 test p-value
Sex							
Male	45 (59.2)	201 (63.0)	204 (62.0)	0.826	0.539	0.652	0.792
Female	31 (40.8)	118 (37.0)	125 (38.0)				
Smoker							
No	35 (46.1)	171 (54.1)	146 (45.2)	0.067	0.206	0.893	0.024
Yes	41 (53.9)	145 (45.9)	177 (54.8)				

Table 6 cont.

Characteristic	Cluster 1 (Non-dippers) (n=77)	Cluster 2 (Moderate dippers) (n=322)	Cluster 3 (Strong dippers) (n=337)	Overall p-value	Cluster 1 vs. Cluster 2	Cluster 1 vs. Cluster 3	Cluster 2 vs. Cluster 3
Alcohol drinker							
No	56 (73.7)	242 (76.3)	241 (73.5)	0.686	0.627	0.970	0.402
Yes	20 (26.3)	75 (23.7)	87 (26.5)				
Diabetes mellitus							
No	57 (75.0)	256 (80.8)	266 (81.1)	0.467	0.263	0.232	0.912
Yes	19 (25.0)	61 (19.2)	62 (18.9)				
Treated hypertension							
No	61 (80.3)	205 (64.7)	250 (76.2)	0.001	0.009	0.451	0.001
Yes	15 (19.7)	112 (35.3)	78 (23.8)				
Cardiovascular disease							
No	67 (88.2)	271 (85.5)	289 (88.1)	0.582	0.547	0.991	0.325
Yes	9 (11.8)	46 (14.5)	39 (11.9)				
Dyslipidemia							
No	57 (75.0)	252 (79.5)	242 (73.8)	0.221	0.391	0.827	0.087
Yes	19 (25.0)	65 (20.5)	86 (26.2)				

Post-hoc pairwise chi-squared tests were adjusted for family-wise error rate. Abbreviations: BMI, body mass index; SD, standard deviation.

TWED-Derived Clusters

Using the CVIs and visual inspection of the series patterns and descriptive statistics (Table 7, Figures 11 & 12), the optimal TWED solution consisted of three clusters with parameters $\nu = 1.0$ and $\lambda = 0.5$. The CVI scores were: silhouette 0.038, Dunn 0.329, Modified Davies–Bouldin 1.501, and Calinski–Harabasz 668.75. The three clusters contained 989, 492, and 674 time series, respectively.

Cluster 2 exhibited the highest nighttime dipping for all three BP measures, along with significantly lower nighttime minimum, maximum, and mean BP than the other two clusters (Table 7, Figures 9, 10, & 13). Cluster 2 also exhibited significantly lower range, SD, COV, ARV, and VIM, both during the daytime and across the recording period as a whole. Nighttime variability in terms of range, SD, COV and VIM was normal or higher for Cluster 2 than the other clusters; however, ARV at night was significantly lower. Cluster 3 had the lowest levels of nighttime dipping, and highest nighttime minimum, maximum, and mean BP levels. Cluster 3 was also associated with high ARV, both during the day and at night. Cluster 1, while often significantly different from the other two clusters, found itself frequently ranked as the middle of the three clusters.

Cluster 3 had the highest levels of nighttime hypertension by all three BP metrics (SBP 82.9%, DBP 70.9%, MAP 76.4%). Cluster 2 had the lowest rates of nighttime hypertension, but these still comprised around half or more of the participants (SBP 65.7%, DBP 49.4%, MAP 53.7%). The distributions of nighttime BP can be seen in Figure 9.

Table 7: Comparison of ABP descriptive statistics across TWED-derived clusters.

Descriptive Statistic	**Cluster 1^ (n = 989)**	**Cluster 2^ (n = 492)**	**Cluster 3^ (n = 674)**	**Cluster 1 vs. Cluster 2**	**Cluster 1 vs. Cluster 3**	**Cluster 2 vs. Cluster 3**
Continuous variable	mean (SE)	mean (SE)	mean (SE)	Tukey-Kramer p-value	Tukey-Kramer p-value	Tukey-Kramer p-value
Dipping DBP	9.2 (0.23)	13.1 (0.33)	3.9 (0.28)	< 0.001	< 0.001	< 0.001
Dipping MAP	7.3 (0.21)	10.7 (0.30)	1.8 (0.26)	< 0.001	< 0.001	< 0.001
Dipping SBP	6.0 (0.20)	8.8 (0.28)	0.6 (0.24)	< 0.001	< 0.001	< 0.001
Maximum DBP	100 (0.41)	99.0 (0.58)	100.5 (0.49)	0.290	0.701	0.095
Maximum DBP (Day)	99.7 (0.40)	98.8 (0.57)	100.1 (0.49)	0.334	0.858	0.184
Maximum DBP (Night)	82.1 (0.41)	81.3 (0.58)	85.1 (0.50)	0.492	< 0.001	< 0.001
Maximum MAP	124.0 (0.49)	121.9 (0.69)	124.7 (0.59)	0.033	0.701	0.008
Maximum MAP (Day)	123.8 (0.49)	121.7 (0.69)	124.0 (0.59)	0.033	0.943	0.025
Maximum MAP (Night)	102.9 (0.48)	100.6 (0.68)	107.8 (0.58)	0.021	< 0.001	< 0.001
Maximum SBP	167.8 (0.74)	163.9 (1.05)	169.6 (0.90)	0.006	0.275	< 0.001
Maximum SBP (Day)	167.5 (0.74)	163.6 (1.05)	168.6 (0.89)	0.007	0.576	0.001
Maximum SBP (Night)	139.3 (0.67)	135.7 (0.95)	147.3 (0.81)	0.006	< 0.001	< 0.001
Mean DBP	73.1 (0.30)	74.1 (0.42)	73.2 (0.36)	0.188	0.993	0.279
Mean DBP (Day)	74.6 (0.30)	76.0 (0.43)	73.8 (0.37)	0.017	0.267	< 0.001
Mean DBP (Night)	67.7 (0.33)	66.1 (0.47)	70.9 (0.40)	0.011	< 0.001	< 0.001
Mean MAP	92.7 (0.35)	93.1 (0.49)	93.6 (0.42)	0.834	0.271	0.725
Mean MAP (Day)	94.1 (0.35)	95.1 (0.49)	93.9 (0.42)	0.267	0.933	0.190
Mean MAP (Night)	87.3 (0.39)	84.8 (0.55)	92.2 (0.47)	0.001	< 0.001	< 0.001
Mean SBP	127.7 (0.51)	127.2 (0.72)	129.6 (0.62)	0.876	0.040	0.033
Mean SBP (Day)	129.3 (0.51)	129.5 (0.72)	129.8 (0.62)	0.968	0.795	0.946
Mean SBP (Night)	121.6 (0.56)	118.0 (0.79)	129.1 (0.67)	0.001	< 0.001	< 0.001
Minimum DBP	52.0 (0.28)	51.1 (0.40)	52.4 (0.34)	0.151	0.733	0.048
Minimum DBP (Day)	54.1 (0.30)	55.6 (0.42)	53.7 (0.36)	0.008	0.699	0.002

Table 7 cont.

Minimum DBP (Night)	55.8 (0.32)	53.2 (0.46)	58.5 (0.39)	< 0.001	< 0.001	< 0.001
Minimum MAP	69.4 (0.33)	68.3 (0.47)	70.0 (0.40)	0.148	0.505	0.020
Minimum MAP (Day)	71.3 (0.34)	72.6 (0.49)	71.1 (0.41)	0.081	0.921	0.053
Minimum MAP (Night)	74.4 (0.38)	71.3 (0.53)	78.7 (0.46)	< 0.001	< 0.001	< 0.001
Minimum SBP	100.8 (0.46)	99.3 (0.65)	101.9 (0.55)	0.163	0.229	0.006
Minimum SBP (Day)	103.2 (0.46)	104.3 (0.66)	103.3 (0.56)	0.333	0.975	0.492
Minimum SBP (Night)	106.4 (0.53)	102.4 (0.75)	112.8 (0.64)	< 0.001	< 0.001	< 0.001
Range DBP	48.0 (0.35)	47.8 (0.50)	48.2 (0.43)	0.965	0.942	0.865
Range DBP (Day)	45.6 (0.35)	43.1 (0.50)	46.3 (0.43)	< 0.001	0.412	< 0.001
Range DBP (Night)	26.2 (0.31)	28.0 (0.44)	26.6 (0.38)	0.003	0.740	0.035
Range MAP	54.6 (0.41)	53.6 (0.58)	54.7 (0.50)	0.305	0.998	0.334
Range MAP (Day)	52.5 (0.41)	49.1 (0.58)	52.9 (0.50)	< 0.001	0.757	< 0.001
Range MAP (Night)	28.4 (0.33)	29.3 (0.47)	29.1 (0.40)	0.246	0.405	0.913
Range SBP	67.0 (0.58)	64.5 (0.82)	67.6 (0.70)	0.035	0.784	0.012
Range SBP (Day)	64.3 (0.58)	59.3 (0.83)	65.3 (0.71)	< 0.001	0.517	< 0.001
Range SBP (Night)	32.9 (0.38)	33.3 (0.54)	34.5 (0.47)	0.819	0.020	0.202
SD DBP	10.3 (0.07)	10.0 (0.10)	10.3 (0.09)	0.038	0.993	0.072
SD DBP (Day)	10.2 (0.07)	9.1 (0.10)	10.4 (0.09)	< 0.001	0.104	< 0.001
SD DBP (Night)	7.7 (0.09)	8.2 (0.12)	7.9 (0.11)	0.001	0.207	0.145
SD MAP	11.5 (0.08)	11.0 (0.11)	11.5 (0.10)	0.001	0.998	0.004
SD MAP (Day)	11.5 (0.08)	10.3 (0.12)	11.7 (0.10)	< 0.001	0.355	< 0.001
SD MAP (Night)	8.3 (0.09)	8.6 (0.13)	8.6 (0.11)	0.252	0.067	0.916
SD SBP	13.6 (0.11)	12.9 (0.16)	13.9 (0.14)	< 0.001	0.199	< 0.001
SD SBP (Day)	13.6 (0.12)	12.1 (0.17)	14.1 (0.14)	< 0.001	0.042	< 0.001
SD SBP (Night)	9.6 (0.11)	9.7 (0.16)	10.3 (0.13)	0.915	< 0.001	0.008
COV DBP	14.2 (0.10)	13.6 (0.14)	14.2 (0.12)	0.001	0.999	0.003
COV DBP (Day)	13.7 (0.10)	12.1 (0.14)	14.2 (0.12)	< 0.001	0.007	< 0.001
COV DBP (Night)	11.4 (0.13)	12.6 (0.18)	11.3 (0.16)	< 0.001	0.730	< 0.001
COV MAP	12.5 (0.08)	11.9 (0.12)	12.4 (0.10)	< 0.001	0.727	0.004

Table 7 cont.

COV MAP (Day)	12.3 (0.09)	10.8 (0.12)	12.5 (0.10)	< 0.001	0.157	< 0.001
COV MAP (Night)	9.6 (0.10)	10.2 (0.15)	9.4 (0.13)	0.002	0.717	< 0.001
COV SBP	10.7 (0.08)	10.1 (0.12)	10.8 (0.10)	< 0.001	0.808	< 0.001
COV SBP (Day)	10.6 (0.09)	9.4 (0.12)	10.9 (0.10)	< 0.001	0.038	< 0.001
COV SBP (Night)	7.9 (0.08)	8.3 (0.12)	8.0 (0.10)	0.078	0.868	0.253
ARV DBP	8.2 (0.05)	8.0 (0.07)	8.5 (0.06)	0.104	0.001	< 0.001
ARV DBP (Day)	6.6 (0.04)	6.4 (0.06)	6.8 (0.05)	0.002	0.004	< 0.001
ARV DBP (Night)	1.9 (0.02)	1.8 (0.03)	2.1 (0.03)	0.085	0.002	< 0.001
ARV MAP	9.0 (0.05)	8.7 (0.08)	9.2 (0.07)	0.010	0.032	< 0.001
ARV MAP (Day)	7.2 (0.05)	6.9 (0.07)	7.4 (0.06)	0.001	0.097	< 0.001
ARV MAP (Night)	2.1 (0.02)	1.9 (0.03)	2.2 (0.03)	< 0.001	0.004	< 0.001
ARV SBP	9.7 (0.06)	9.4 (0.08)	10.1 (0.07)	0.009	0.001	< 0.001
ARV SBP (Day)	7.8 (0.05)	7.5 (0.07)	8.0 (0.06)	0.003	0.010	< 0.001
ARV SBP (Night)	2.4 (0.03)	2.1 (0.04)	2.5 (0.03)	< 0.001	< 0.001	< 0.001
VIM DBP	10.3 (0.07)	10.0 (0.10)	10.3 (0.08)	0.006	0.993	0.015
VIM DBP (Day)	10.2 (0.07)	9.1 (0.10)	10.5 (0.09)	< 0.001	0.034	< 0.001
VIM DBP (Night)	7.7 (0.09)	8.4 (0.12)	7.8 (0.10)	< 0.001	0.839	0.001
VIM MAP	11.5 (0.08)	11.0 (0.11)	11.5 (0.09)	< 0.001	0.845	0.003
VIM MAP (Day)	11.5 (0.08)	10.2 (0.11)	11.7 (0.10)	< 0.001	0.210	< 0.001
VIM MAP (Night)	8.4 (0.09)	8.8 (0.13)	8.4 (0.11)	0.017	0.923	0.066
VIM SBP	13.7 (0.10)	12.9 (0.15)	13.8 (0.13)	< 0.001	0.695	< 0.001
VIM SBP (Day)	13.7 (0.11)	12.1 (0.16)	14.1 (0.13)	< 0.001	0.038	< 0.001
VIM SBP (Night)	9.7 (0.10)	10.1 (0.15)	9.9 (0.12)	0.155	0.482	0.735
Categorical variable	n (%)	n (%)	n (%)	χ^2 p-value	χ^2 p-value	χ^2 p-value
Hypertensive SBP	477 (48.2)	236 (48.0)	362 (54.4)	0.924	0.045	0.064
Hypertensive SBP (Day)	397 (40.1)	202 (41.1)	283 (42.5)	1.000	1.000	1.000
Hypertensive SBP (Night)	754 (76.2)	323 (65.7)	552 (82.9)	< 0.001	0.001	< 0.001
Hypertensive DBP	334 (33.8)	191 (38.8)	245 (36.8)	0.168	0.414	0.480
Hypertensive DBP (Day)	221 (22.3)	146 (29.7)	151 (22.7)	0.006	0.876	0.014

Table 7 cont.

Hypertensive DBP (Night)	584 (59.0)	243 (49.4)	472 (70.9)	< 0.001	< 0.001	< 0.001
Hypertensive MAP	437 (44.2)	227 (46.1)	330 (49.5)	0.502	0.096	0.502
Hypertensive MAP (Day)	328 (33.2)	200 (40.7)	242 (36.3)	0.015	0.270	0.270
Hypertensive MAP (Night)	651 (65.8)	264 (53.7)	509 (76.4)	< 0.001	< 0.001	< 0.001
Dipping SBP				< 0.001	< 0.001	< 0.001
Reverse (≤ 0)	177 (17.9)	34 (6.9)	356 (53.5)			
Non- (> 0 to ≤ 10)	641 (64.8)	284 (57.7)	264 (39.6)			
Normal (> 10 to ≤ 20)	162 (16.4)	168 (34.1)	46 (6.9)			
Extreme (> 20)	9 (0.9)	6 (1.2)	0 (0.0)			
Dipping DBP				< 0.001	< 0.001	< 0.001
Reverse (≤ 0)	113 (11.4)	16 (3.3)	269 (40.4)			
Non- (> 0 to ≤ 10)	501 (50.7)	172 (35.0)	259 (38.9)			
Normal (> 10 to ≤ 20)	322 (32.6)	240 (48.8)	126 (18.9)			
Extreme (> 20)	53 (5.4)	64 (13.0)	12 (1.8)			
Dipping MAP				< 0.001	< 0.001	< 0.001
Reverse (≤ 0)	146 (14.8)	28 (5.7)	326 (48.9)			
Non- (> 0 to ≤ 10)	589 (59.6)	237 (48.2)	262 (39.3)			
Normal (> 10 to ≤ 20)	237 (24.0)	202 (41.1)	74 (11.1)			
Extreme (> 20)	17 (1.7)	25 (5.1)	4 (0.6)			

Abbreviations: ARV, average real variability; COV, coefficient of variation; DBP, diastolic blood pressure; MAP, mean arterial pressure; SBP, systolic blood pressure; SD, standard deviation; SE, standard error; VIM, variability independent of the mean.
Green fill denotes cluster with highest value where significantly different from the other two clusters. Red fill denotes cluster with lowest value where significantly different from the other two clusters.

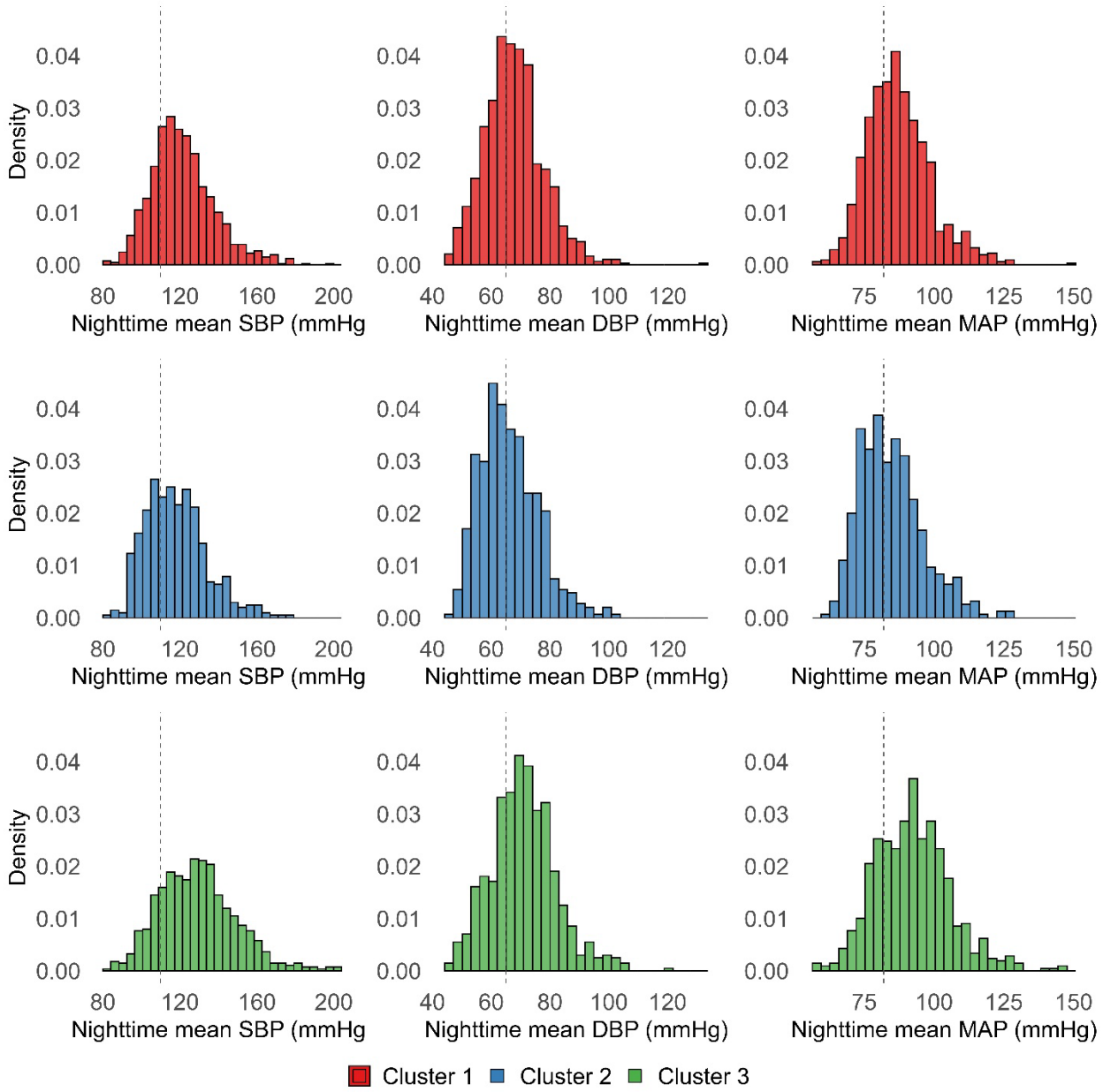

Figure 9: Histograms of nighttime mean DBP, MAP and SBP for TWED-derived clusters. Dotted lines denote respective hypertension thresholds. Abbreviations: DBP, diastolic blood pressure; MAP, mean arterial pressure; SBP, systolic blood pressure; TWED, time warp edit distance.

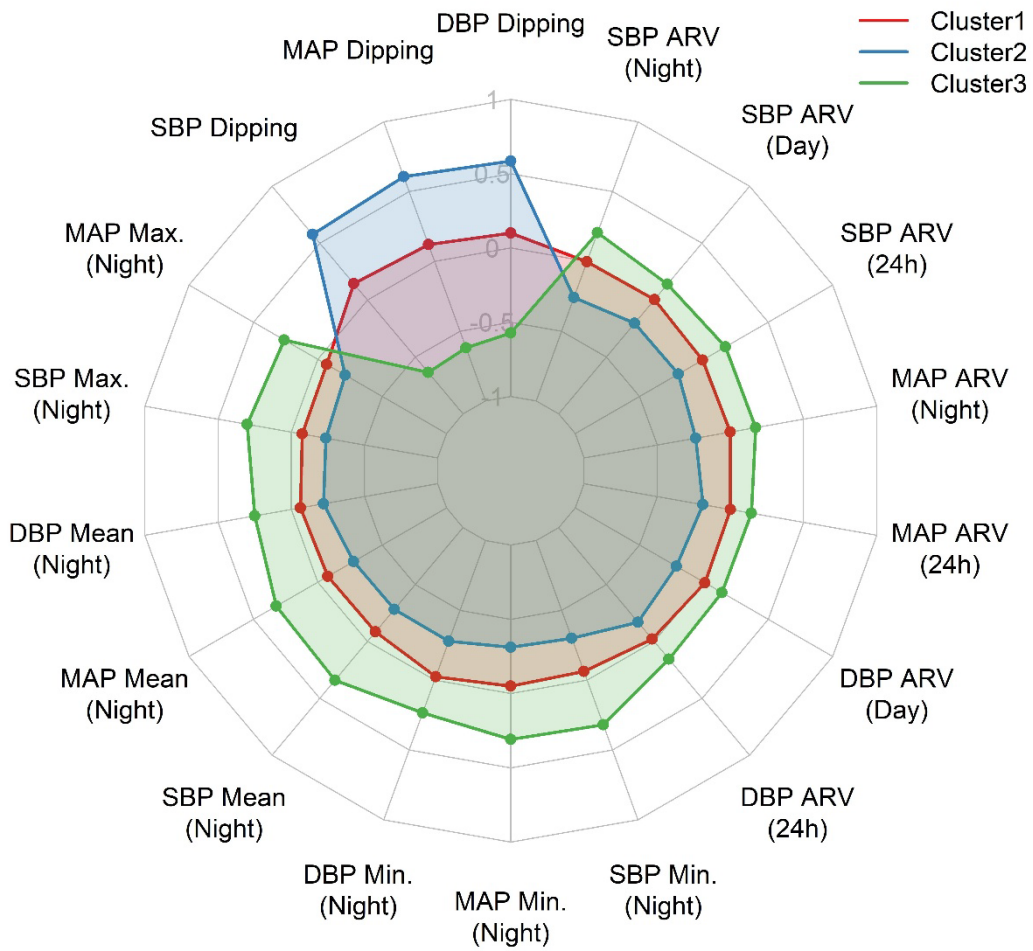

Figure 10: Radar chart showing standardized values for significantly different continuous ABP variables across TWED-derived clusters. Abbreviations: ABP, ambulatory blood pressure; ARV, average real variability; DBP, diastolic blood pressure; MAP, mean arterial pressure; SBP, systolic blood pressure; TWED, time warp edit distance.

As seen in Figure 11, all three clusters share a similar general shape with a dip in the afternoon that bottoms out somewhere between 14:00 and 16:00 then begins rising until a peak around 19:00. Cluster 2 then drops the most dramatically down to a low around 02:00. Cluster 3 stops falling around 22:00 and climbs steadily throughout the night, while Cluster 1 sits in between, settling around 0.5 standard deviations below its mean for much of the night before rising sharply after 04:00. The multidimensional scaling plot in Figure 12 shows Cluster 2 and Cluster 3 well separated, with Cluster 1 in between.

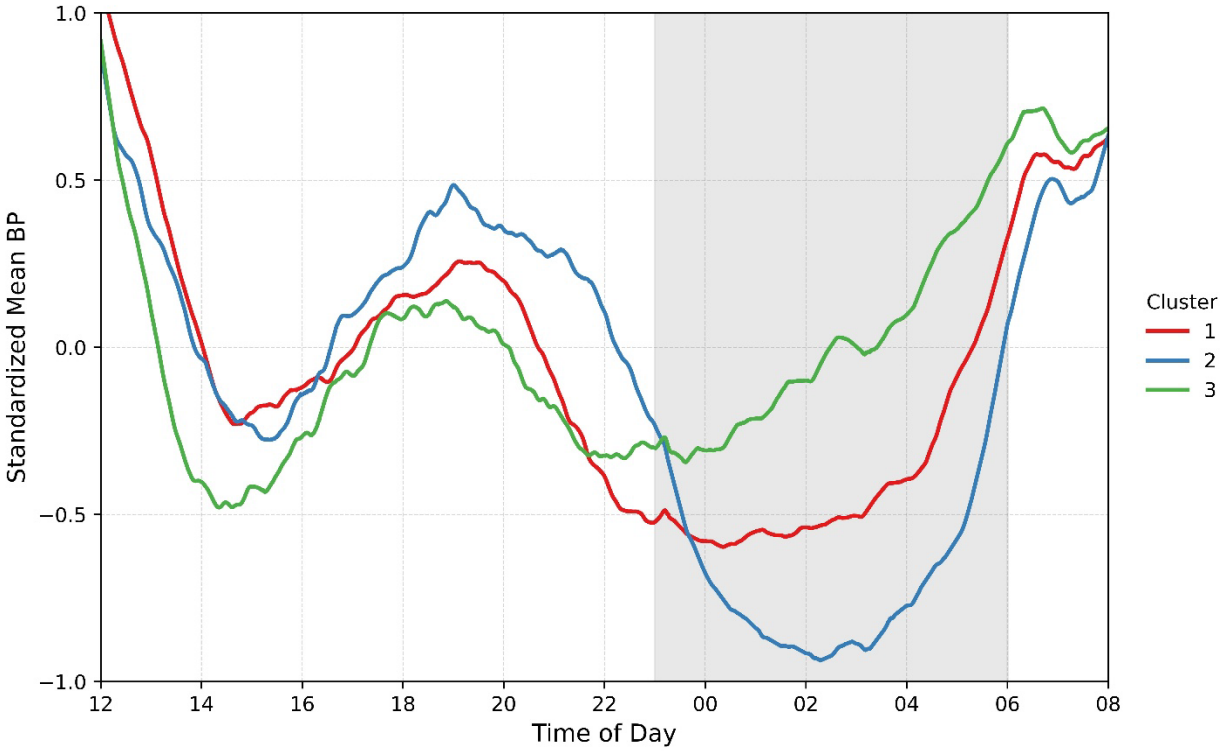

Figure 11: Loess-smoothed series means for TWED-derived clusters. The line for each cluster represents the mean of the standardized values for SBP, DBP and MAP at each timepoint. Designated nighttime hours are marked with gray background. Abbreviations: BP, blood pressure; DBP, diastolic blood pressure; MAP, mean arterial pressure; SBP, systolic blood pressure; TWED, time warp edit distance.

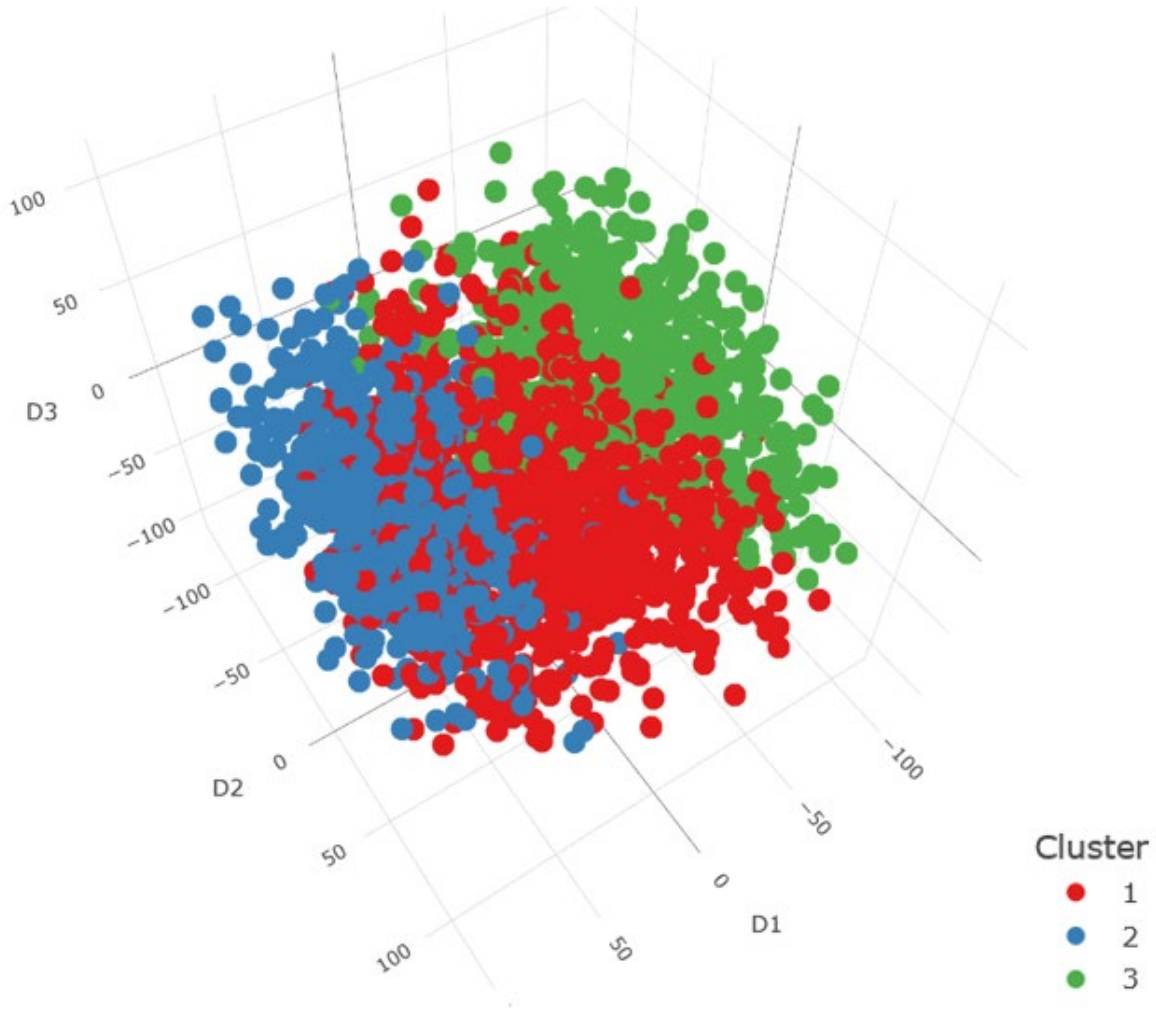

Figure 12: Multidimensional scaling (3D) representation of TWED-derived clusters.

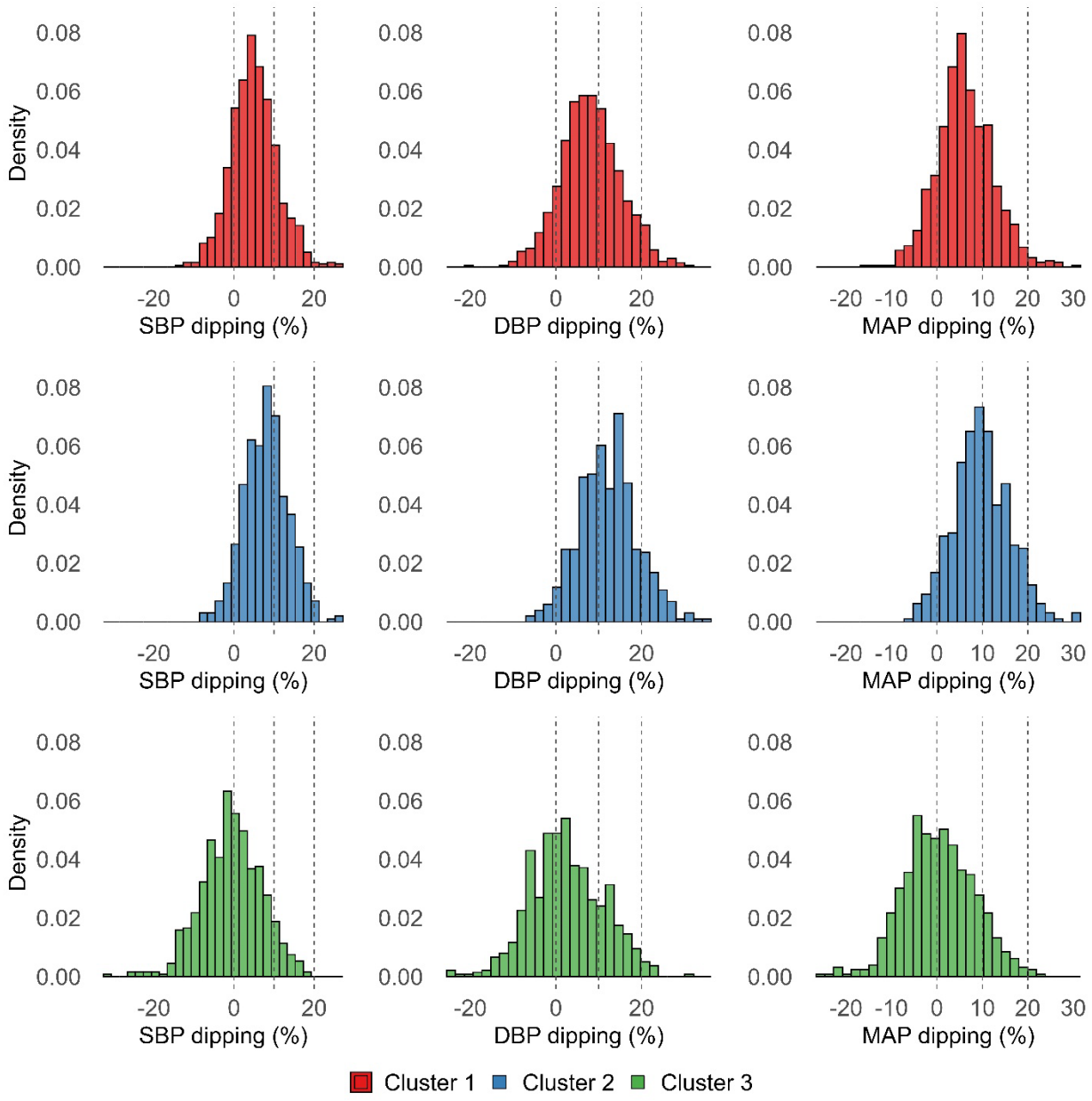

Figure 13: Histograms of DBP, MAP and SBP dipping % for TWED-derived clusters. Dotted lines denote dipping thresholds. Reverse dipping < 0; non-dipping ≥ 0 to < 10; normal dipping ≥ 10 to < 20; extreme dipping ≥ 20. Abbreviations: DBP, diastolic blood pressure; MAP, mean arterial pressure; SBP, systolic blood pressure; TWED, time warp edit distance.

Table 8: Characterization of TWED-derived clusters.

Cluster	Characterization	Pattern Summary	Clinical Interpretation
1	"Moderate dippers"	Moderate dipping in SBP, DBP, and MAP, with midrange variability values.	Typical circadian BP rhythm with nocturnal hypertension and moderate cardiovascular and cognitive risk.
2	"Strong dippers"	Greatest nighttime BP decline, low 24h and daytime variability, higher variability at night but low nighttime ARV.	Normal or extreme dipping pattern with favorable cardiovascular and cognitive profile.
3	"Non-dippers"	Minimal or reversed nighttime dipping, elevated nighttime BP levels, and higher daytime variability and night ARV.	Nocturnal hypertension or reverse dipping pattern associated with increased cardiovascular and cognitive risk.

Abbreviations: ARV, average real variability; BP, blood pressure; DBP, diastolic blood pressure; MAP, mean arterial pressure; SBP, systolic blood pressure.

The same 736 patients were used for baseline analysis as were used in the DTW clusters. In the comparison of baseline characteristics between TWED clusters, only age and education were found to have a significant overall difference among the clusters (Table 9). Following a similar pattern to the DTW clusters, the strong dippers' cluster, which had significantly the lowest mean age (62.81 years; SD 6.27), also had significantly the highest mean number of years of education (7.68 years; SD 4.04). Strong dippers additionally had the highest mean score in all five cognitive tests. The scores for Stein minimental and total memory were found to have significant overall differences between the clusters from a one-way ANOVA test. Only total memory had a significant pairwise difference, between strong dippers (mean score 39.95) and moderate dippers (37.75).

Table 9: Comparison of baseline socio-demographic and clinical characteristics between TWED-derived clusters.

Variable	**Cluster 1 (Moderate dippers) (n = 383)**	**Cluster 2 (Strong dippers) (n = 165)**	**Cluster 3 (Non-dippers) (n = 188)**	**Overall p-value**	**Cluster 1 vs. Cluster 2**	**Cluster 1 vs. Cluster 3**	**Cluster 2 vs. Cluster 3**
Continuous variable	mean (SD)	mean (SD)	mean (SD)	ANOVA F-test p-value	Tukey-Kramer p-value	Tukey-Kramer p-value	Tukey-Kramer p-value
Age (years)	65.42 (7.55)	62.81 (6.27)	65.67 (7.88)	<0.001	< 0.001	0.923	0.001
Education (years)	6.55 (4.16)	7.68 (4.04)	6.18 (3.97)	0.002	0.009	0.562	0.002
Weight (kg)	67.36 (13.17)	69.21 (14.10)	69.42 (13.84)	0.154	0.316	0.212	0.988
Height (m)	1.58 (0.09)	1.59 (0.09)	1.57 (0.09)	0.281	0.310	0.987	0.340
BMI (kg/m^2)	27.11 (4.72)	27.41 (4.96)	27.99 (5.00)	0.134	0.779	0.110	0.515
Serum glucose (mg/dL)	110.11 (46.88)	120.91 (67.63)	111.51 (46.14)	0.224	0.199	0.969	0.402
Total cholesterol (mg/dL)	190.43 (53.50)	186.37 (54.34)	194.69 (75.84)	0.617	0.843	0.807	0.588
Triglycerides (mg/dL)	157.07 (98.80)	170.07 (118.09)	169.47 (126.13)	0.478	0.595	0.588	0.999
Stein minimental	44.43 (7.44)	45.91 (7.34)	44.10 (7.26)	0.047	0.080	0.876	0.058
Folstein minimental	24.10 (3.99)	24.75 (3.91)	24.03 (3.75)	0.155	0.181	0.979	0.205
Total memory	37.75 (9.40)	39.95 (8.77)	38.19 (9.28)	0.039	0.031	0.860	0.178
Short term memory	5.32 (2.29)	5.73 (2.04)	5.46 (2.22)	0.139	0.114	0.758	0.487
Long term memory	24.01 (11.68)	26.20 (12.03)	24.66 (11.64)	0.142	0.117	0.813	0.444
Sex							
Male	243 (64.5)	90 (55.2)	117 (63.6)	0.114	0.043	0.840	0.113
Female	134 (35.5)	73 (44.8)	67 (36.4)				
Smoker							
No	193 (51.7)	67 (42.1)	92 (50.3)	0.121	0.042	0.745	0.132
Yes	180 (48.3)	92 (57.9)	91 (49.7)				
Alcohol drinker							

Variable	Cluster 1 (Moderate dippers) (n = 383)	Cluster 2 (Strong dippers) (n = 165)	Cluster 3 (Non-dippers) (n = 188)	Overall p-value	Cluster 1 vs. Cluster 2	Cluster 1 vs. Cluster 3	Cluster 2 vs. Cluster 3
No	286 (76.1)	113 (69.8)	140 (76.5)	0.248	0.125	0.909	0.157
Yes	90 (23.9)	49 (30.2)	43 (23.5)				
Diabetes mellitus							
No	301 (80.1)	133 (82.1)	145 (79.2)	0.788	0.582	0.821	0.502
Yes	75 (19.9)	29 (17.9)	38 (20.8)				
Treated hypertension							
No	271 (72.1)	121 (74.7)	124 (67.8)	0.345	0.531	0.293	0.157
Yes	105 (27.9)	41 (25.3)	59 (32.2)				
Cardiovascular disease							
No	326 (86.7)	146 (90.1)	155 (84.7)	0.320	0.267	0.521	0.132
Yes	50 (13.3)	16 (9.9)	28 (15.3)				
Dyslipidemia							
No	289 (76.9)	126 (77.8)	136 (74.3)	0.720	0.816	0.508	0.453
Yes	87 (23.1)	36 (22.2)	47 (25.7)				

Abbreviations: BMI, body mass index; SD, standard deviation.

Table 10 compares baseline patients' membership of clusters between the DTW and TWED methods. For each of the DTW clusters, more than 50% of patients in that cluster were in the same TWED cluster. In the DTW non-dippers, 57.1% (n = 44) of patients were in the TWED non-dippers. In the DTW moderate dippers, 58.4% (n = 188) were in the moderate dippers from TWED. And from DTW's strong dipping cluster, 52.5% (n = 169) also found themselves in the TWED moderate dippers. A chi-squared test of independence found that the two sets of clusters are statistically unlikely to be independent (χ^2 = 139.56 on 4 degrees of freedom; $p < 0.001$).

Table 10: Comparison of DTW and TWED cluster membership among baseline patients.

	DTW Cluster 1 (Non-dippers)	**DTW Cluster 2 (Moderate dippers)**	**DTW Cluster 3 (Strong dippers)**	**Total**
	n (%)	n (%)	n (%)	n (%)
TWED Cluster 1 (Moderate dippers)	26 (33.8)	188 (58.4)	169 (52.5)	383 (52.0)
TWED Cluster 2 (Strong dippers)	7 (9.1)	29 (9.0)	129 (40.1)	165 (22.4)
TWED Cluster 3 (Non-dippers)	44 (57.1)	105 (32.6)	39 (12.1)	188 (25.6)
Total	77 (100)	322 (100)	337 (100)	736 (100)

Abbreviations: DTW, dynamic time warping; TWED, time warp edit distance.

A similar comparison is shown in Table 11 involving all 2,147 time series that were used in the two clustering methods. Again, the majority of series from the DTW non-dipping cluster were also in the TWED non-dippers (n = 211, 60.5%). For both the DTW moderate dippers (n = 463, 53.5%) and strong dippers (n = 425, 45.6%), the most common TWED cluster was the moderate dipping cluster. The chi-squared test of independence also found that independence between the two sets of clusters was unlikely (χ^2 = 404.37 on 4 degrees of freedom; $p < 0.001$).

Table 11: Comparison of DTW and TWED cluster membership among all ABPM time series.

	DTW Cluster 1 (Non-dippers)	**DTW Cluster 2 (Moderate dippers)**	**DTW Cluster 3 (Strong dippers)**	**Total**
	n (%)	n (%)	n (%)	n (%)
TWED Cluster 1 (Moderate dippers)	101 (28.9)	463 (53.5)	425 (45.6)	989 (46.1)
TWED Cluster 2 (Strong dippers)	37 (10.6)	89 (10.3)	366 (39.2)	492 (22.9)
TWED Cluster 3 (Non-dippers)	211 (60.5)	313 (36.2)	142 (15.2)	666 (31.0)
Total	349 (100)	865 (100)	933 (100)	2147 (100)

Abbreviations: ABPM, ambulatory blood pressure monitoring; DTW, dynamic time warping; TWED, time warp edit distance.

CHAPTER V

DISCUSSION

The primary objectives of this study were to compare DTW and TWED time-series clustering methods for characterizing 24-hour ABP patterns and to assess the clinical relevance of the resulting clusters. Both the DTW and TWED clustering algorithms identified distinct circadian BP phenotypes. Yim & Ramdeen (2015) point out that clustering algorithms will cluster the data regardless; it does not always mean the clusters are meaningful unless interpretation and significance of the clusters are given correctly by the researcher. The quality of these clusters was supported by internal validation metrics and the concordance of two different algorithms, as well as prior research. Notably, cluster membership was not identical between the DTW and TWED solutions – roughly 50 to 60% of individuals in a given DTW cluster were found in the analogous TWED cluster. This partial overlap suggests that while both methods identify similar broad phenotypes, they differ in how borderline cases are assigned.

Despite the differences between the DTW and TWED methods, a similar three-cluster structure emerged from both approaches. Most notably, one group exhibited a large nighttime dip in BP with the lowest rates of nighttime hypertension, a second group showed a moderate dip, and a third group displayed either no dip or a reverse dipping pattern with the highest incidence of nocturnal hypertension. The clusters also differed markedly in BP variability measures. In the DTW-derived clusters, nighttime COV and VIM were elevated in the strong-dipping group, whereas nighttime ARV was lower than the other clusters. This highlights the influence of structured diurnal change on standard variability metrics: when nighttime dipping is

pronounced, the magnitude of BP variation relative to the overall mean can increase, even if short-term fluctuations are minimal. Similar findings have been reported by Japie et al. (2016) and Hernandez & Chang (2023), who emphasized that 24-hour SD and COV are strongly driven by mean BP and the day-night amplitude, conflating physiologic circadian variation with pathological instability. In the TWED-derived clusters, the strong dipping cluster was again associated with high nighttime COV and VIM but low nighttime ARV. However, the non-dipping cluster was associated with higher ARV in the day and night. This may suggest that TWED's sensitivity to temporal irregularity can capture more subtle interval-to-interval fluctuations not fully reflected in the DTW results. The contrast between ARV and the other variability measures is interesting, since recent evidence has suggested that short-term BP variability, rather than overall 24-hour dispersion, carries independent prognostic significance. A meta-analysis by Mena et al. (2017) found that each 1-SD increase in systolic ARV corresponded to an 18% higher risk of cardiovascular events, even after adjusting for mean BP. Similarly, Sible and Nation (2024) found that elevated 24-hour and daytime ARV predicted dementia in older adults under standard BP treatment, while the mean BP level itself was not predictive. The Maracaibo Aging Study further demonstrated that increases in 24-hour and nighttime BP variability over time, rather than mean BP, were associated with cognitive decline (Melgarejo et al., 2024). The divergence between the two methods demonstrates that BP variability is not a single construct but a broad term encompassing both overall BP directional trends and short-term instability (Schutte et al., 2022; Hernandez & Chang, 2023). Traditional variability measures can therefore be misleading when interpreted in isolation: a high 24-hour SD may simply indicate healthy dipping, whereas elevated nighttime ARV more plausibly reflects impaired circadian regulation (Candemir et al., 2022; Kanegusuku et al., 2017).

Across both clustering approaches, modest but consistent differences in baseline characteristics were observed among the derived groups. In the DTW clusters, age, education, triglycerides, and treated hypertension differed significantly, while in the TWED clusters, only age and education showed significant variation. Participants in the strong dipping clusters tended to be somewhat younger and more educated, consistent with previous reports that socioeconomic and behavioral factors influence circadian BP regulation (Sible & Nation, 2024; Gavriilaki et al., 2023). The relationship between dipping pattern and cognitive performance differed by clustering method. In the DTW analysis, the non-dipping cluster showed the highest mean scores but the differences were not statistically significant; whereas in the TWED analysis, the strong-dipping cluster had the highest scores on all five cognitive measures, two of which were significantly higher. This finding is noteworthy given the association of lower nocturnal ARV (alongside higher COV and VIM) in the TWED strong dippers. Prior longitudinal research has shown that lower nighttime variability is associated with better cognitive outcomes (Melgarejo et al., 2024; Sible & Nation, 2024; Gavriilaki et al., 2023).

The three different ABP profiles found by the two methods used in this study align with different BP risk profiles established by prior research into hypertension. Numerous studies have demonstrated that reduced or absent nocturnal BP dipping is associated with higher cardiovascular risk, reduced cognitive function, and other adverse outcomes. In the nationwide JAMP study, Kario et al. (2020) reported that hypertensive adults with a “riser” pattern had more than double the risk of heart failure relative to normal dippers, even after adjustment for mean nighttime BP. Similarly, Yang et al. (2019) found that elevated nighttime systolic BP was a stronger predictor of all-cause and cardiovascular mortality than either daytime or office BP. From a cerebrovascular standpoint, Xu et al. (2021) showed that stroke survivors with sustained

nocturnal hypertension had markedly higher recurrence risk, while Chesebro et al. (2020) demonstrated that reverse dippers exhibited greater white-matter hyperintensity burden and poorer memory performance. A meta-analysis by Gavriilaki et al. (2023) further supports this link, finding that normal dippers had roughly half the risk of cognitive impairment and one-sixth the risk of dementia compared with reverse dippers. In the present study, both DTW and TWED identified the strong-dipping cluster as significantly younger and more highly educated than the other two clusters. Although cognitive scores did not differ significantly across DTW clusters, the TWED results showed significant differences for the Stein minimental and total memory tests, with the strong dippers achieving the highest mean scores on these and all other cognitive measures. Collectively, these findings align with the notion that nocturnal BP fall represents a positive prognostic marker for cardiovascular and cognitive health (Asayama et al., 2023; Huang et al., 2021).

When comparing the two clustering approaches, both DTW and TWED successfully identified interpretable 24-hour BP phenotypes with broadly similar patterns, and comparable CVIs. Both methods identified age and education as significant differences between the strong-dipping clusters and the others, while the TWED method additionally found the strong dippers to have performed significantly better in the cognitive tests. TWED also found a more clear difference in variability: the strong dippers had low short-term variability at night, while the non-dippers had high variability both during the day and at night. While the differences between the two methods are modest, cumulatively these factors give the TWED clusters greater clinical interpretability than DTW. Furthermore, from a methodological standpoint, DTW aligns sequences based solely on their ordering and ignores the actual time intervals, which can lead to unrealistic stretching or compression of points in time. In contrast, TWED incorporates time

information directly, penalizes gaps and temporal mismatches, and manages unevenly sampled or noisy series more effectively through its deletion and insertion operations. Therefore, based on the overall findings of this study, TWED would seem to have a slight edge over DTW.

The methodological robustness of the present study is supported by the general convergence of the DTW and TWED results, which revealed comparable three-cluster structures with consistent circadian BP patterns despite differing sensitivity to variability features. Nonetheless, several limitations warrant consideration. Results may have been influenced by methodological choices such as interpolation or parameter tuning, which can affect variability metrics (Hernandez & Chang, 2023). Additionally, residual confounding from unmeasured factors such as sleep quality, physical activity, or medication adherence cannot be excluded. The use of a 20-hour analysis window, while improving temporal alignment across series, may have excluded certain early-morning surges with potential prognostic significance (Chia et al., 2022; Kario et al., 2020). Finally, the clustering was performed using all available longitudinal patient data, while the clusters associations analyses were focused only on participants' baseline socio-demographic and clinical characteristics. Future research will examine how the derived clusters relate longitudinally to the development of diseases and health conditions.

Conclusions

Clustering 24-hour ABP time series with elastic distance measures (DTW and TWED) proved effective in identifying meaningful ABP patterns that extend beyond feature-based summaries. Both methods delineated three phenotypes – from healthy circadian dipping to pathologic reverse dipping – that are clinically interpretable and backed by known prognostic literature. These findings reinforce calls in hypertension research to look beyond static BP measures or variability metrics such as SD, COV, and ARV, which are only fully interpretable

alongside time-series–based analysis methods for patient risk stratification (Huang et al., 2021; Schutte et al., 2022). This study demonstrates the potential of unsupervised time-series clustering to contribute to enhanced precision in hypertension phenotyping and inform future research into blood pressure and associated health outcomes.

REFERENCES

Aach, J., & Church, G. M. (2001). Aligning gene expression time series with time warping algorithms. *Bioinformatics, 17*(6), 495–508. https://doi.org/10.1093/bioinformatics/17.6.495

Aggarwal, C. C., Hinneburg, A., & Keim, D. A. (2001). On the surprising behavior of distance metrics in high dimensional space. In *International conference on database theory* (pp. 420-434). Springer. https://doi.org/10.1007/3-540-44503-X_27

Alqahtani, A., Ali, M., Xie, X., & Jones, M. W. (2021). Deep time-series clustering: A review. *Electronics, 10*(23), 3001. https://doi.org/10.3390/electronics10233001

Asayama, K., Stolarz-Skrzypek, K., Yang, W.-Y., Hansen, T. W., Brguljan-Hitij, J., Odili, A. N., Li, Y., & Staessen, J. A. (2023). What did we learn from the International Databases on Ambulatory and Home Blood Pressure in Relation to Cardiovascular Outcome? *Hypertension Research, 46*(5), 934–949. https://doi.org/10.1038/s41440-023-01191-4

Aristizábal-Ocampo, D., Álvarez-Montoya, D., Madrid-Muñoz, C., Fernández-Ruiz, R., & Gallo-Villegas, J. (2025). Circulatory phenotypes in hypertension identified by 24-h ambulatory blood pressure monitoring. *Journal of Hypertension.* https://doi.org/10.1097/HJH.0000000000004149

Asmuje, N. F., Mat, S., Goh, C. H., Myint, P. K., & Tan, M. P. (2022). Increased beat-to-beat blood pressure variability is associated with impaired cognitive function. *American Journal of Hypertension, 35*(12), 998–1005. https://doi.org/10.1093/ajh/hpac107

Bellman, R., & Kalaba, R. (1959). On adaptive control processes. *IRE Transactions on Automatic Control, 4*(2), 1–9. https://doi.org/10.1109/TAC.1959.1104847

Berndt, D. J., & Clifford, J. (1994). Using dynamic time warping to find patterns in time series. In *Proceedings of the 3rd international conference on knowledge discovery and data mining* (pp. 359–370). AAAI Press.

Candemir, M., Kiziltunç, E., Candemir, B., Nurkoç, S., Cihan, B., & Şahinarslan, A. (2022). Analysis of ambulatory blood pressure monitoring data in patients with ankylosing spondylitis without clinically evident cardiovascular disease. *Journal of Human Hypertension, 36*(6), 531–536. https://doi.org/10.1038/s41371-021-00542-3

Chesebro, A. G., Melgarejo, J. D., Leendertz, R., Igwe, K. C., Lao, P. J., Laing, K. K., Rizvi, B., Budge, M., Meier, I. B., Calmon, G., Lee, J. H., Maestre, G. E., & Brickman, A. M. (2020). White matter hyperintensities mediate the association of nocturnal blood pressure with cognition. *Neurology, 94*(17), e1803–e1810. https://doi.org/10.1212/WNL.0000000000009316

Chia, J., Bhatia, K. S., Mihailidou, A. S., & Kanagaratnam, L. B. (2022). The role of ambulatory blood pressure monitoring in current clinical practice. *Heart, Lung and Circulation, 31*(10), 1333–1340. https://doi.org/10.1016/j.hlc.2022.06.670

Cleveland Clinic. (2023, March 6). *24-hour ambulatory blood pressure monitoring*. https://my.clevelandclinic.org/health/diagnostics/16330-24-hour-ambulatory-blood-pressure-monitoring

Ester, M., Kriegel, H. P., Sander, J., & Xu, X. (1996, August). A density-based algorithm for discovering clusters in large spatial databases with noise. In Simoudis, E., Han, J., Fayyad, U. (Eds.), *KDD '96: Proceedings of the Second International Conference on Knowledge Discovery and Data Mining* (pp. 226-231). AAAI.

Gavriilaki, M., Anyfanti, P., Mastrogiannis, K., Gavriilaki, E., Lazaridis, A., Kimiskidis, V., & Gkaliagkousi, E. (2023). Association between ambulatory blood pressure monitoring patterns with cognitive function and risk of dementia: A systematic review and meta-analysis. *Aging Clinical and Experimental Research, 35*(3), 745–761. https://doi.org/10.1007/s40520-023-02361-7

Gil, M., Alliey-Rodriguez, N., Lopez-Alvarenga, J. C., Diego, V., Gaona, C. A., Mata, L., Pirela, R. V., Chavez, C. A., de Erausquin, G. A., Melgarejo, J. D., Maestre, G. E. (2021). Neuropsychiatric symptoms among Hispanics: Results of the Maracaibo Aging Study. *Journal of Alzheimer's Disease, 82*(s1), S251–S261. https://doi.org/10.3233/JAD-201144

Giorgino, T. (2009). Computing and visualizing dynamic time warping alignments in R: The dtw package. *Journal of Statistical Software, 31*(7), 1–24. https://doi.org/10.18637/jss.v031.i07

Groppelli, A., Omboni, S., Parati, G., & Mancia, G. (1992). Evaluation of noninvasive blood pressure monitoring devices Spacelabs 90202 and 90207 versus resting and ambulatory 24-hour intra-arterial blood pressure. *Hypertension, 20*(2), 227–232. https://doi.org/10.1161/01.HYP.20.2.227

Guo, Q., Lu, X., Gao, Y., Zhang, J., Yan, B., Su, D., Song, A., Zhao, X., & Wang, G. (2017). Cluster analysis: A new approach for identification of underlying risk factors for coronary artery disease in essential hypertensive patients. *Scientific Reports, 7*, 43965. https://doi.org/10.1038/srep43965

Hernandez, M. F., & Chang, T. I. (2023). The need to reduce variability in the study of blood pressure variability. *American Journal of Kidney Diseases, 81*(4), 379–381. https://doi.org/10.1053/j.ajkd.2022.10.008

Holder, C., Middlehurst, M., & Bagnall, A. (2024). A review and evaluation of elastic distance functions for time series clustering. *Knowledge and Information Systems, 66*(3), 765–809. https://doi.org/10.1007/s10115-023-01952-0

Huang, Q.-F., Yang, W.-Y., Asayama, K., Zhang, Z.-Y., Thijs, L., Li, Y., O'Brien, E., & Staessen, J. A. (2021). Ambulatory blood pressure monitoring to diagnose and manage hypertension. *Hypertension, 77*(2), 254–264. https://doi.org/10.1161/HYPERTENSIONAHA.120.14591

Hyun, M. H., Kang, J. H., Kim, S., Na, J. O., Choi, C. U., Kim, J. W., Kim, E. J., Rha, S.-W., Park, C. G., Lee, E., & Seo, H. S. (2020). Patterns of circadian variation in 24-hour ambulatory blood pressure, heart rate, and sympathetic tone correlate with cardiovascular disease risk: A cluster analysis. *Cardiovascular Therapeutics, 2020*(1). https://doi.org/10.1155/2020/4354759

Japie, C., Weiss, E., Bunea, M., Frunza, S., Daraban, A. M., Bartos, D., & Badila, E. (2016). From clinical considerations to theory - Blood pressure variability profiles and patterns. *Mædica – A Journal of Clinical Medicine, 11*(2), 101–108. https://pmc.ncbi.nlm.nih.gov/articles/PMC5394576/

Jia, D., Zhang, D., & Li, N. (2014). Pulse waveform classification using support vector machine with Gaussian time warp edit distance kernel. *Computational and Mathematical Methods in Medicine, 2014*(1). https://doi.org/10.1155/2014/947254

Kanegusuku, H., Silva-Batista, C., Peçanha, T., Silva-Junior, N., Queiroz, A., Costa, L., Mello, M., Piemonte, M., Ugrinowitsch, C., & Forjaz, C. (2017). Patients with Parkinson disease present high ambulatory blood pressure variability. *Clinical Physiology and Functional Imaging, 37*(5), 530–535. https://doi.org/10.1111/cpf.12338

Kario, K., Hoshide, S., Mizuno, H., Kabutoya, T., Nishizawa, M., Yoshida, T., Abe, H., Katsuya, T., Fujita, Y., Okazaki, O., Yano, Y., Tomitani, N., & Kanegae, H. (2020). Nighttime blood pressure phenotype and cardiovascular prognosis: Practitioner-based nationwide JAMP study. *Circulation, 142*(19), 1810–1820. https://doi.org/10.1161/CIRCULATIONAHA.120.049730

Keogh, E., & Ratanamahatana, C. A. (2005). Exact indexing of dynamic time warping. *Knowledge and Information Systems, 7*(3), 358–386. https://doi.org/10.1007/s10115-004-0154-9

Kohonen, T. (2002). The self-organizing map. *Proceedings of the IEEE*, *78*(9), 1464-1480. https://doi.org/10.1109/5.58325

Lemire, D. (2009). Faster retrieval with a two-pass dynamic-time-warping lower bound. *Pattern Recognition, 42*(9), 2169–2180. https://doi.org/10.1016/j.patcog.2008.11.030

Li, H., Wan, X., Liang, Y., & Gao, S. (2014). Dynamic time warping based on cubic spline interpolation for time series data mining. In *Proceedings of the 2014 IEEE International Conference on Data Mining Workshop* (pp. 19–26). IEEE. https://doi.org/10.1109/ICDMW.2014.21

Lin, J., Williamson, S., Borne, K., & DeBarr, D. (2012). Pattern recognition in time series. In M. J. Way, J. D. Scargle, K. M. Ali, & A. N. Srivastava (Eds.), *Advances in machine learning and data mining for astronomy* (pp.617-645). Routledge.

Liu, L., Zuo, W., Zhang, D., Li, N., & Zhang, H. (2010). Classification of wrist pulse blood flow signal using time warp edit distance. In D. Zhang & M. Sonka (Eds.), *Proceedings of the International Conference on Medical Biometrics (ICMB 2010), Lecture Notes in Computer Science* (Vol. 6165, pp. 137–144). Springer. https://doi.org/10.1007/978-3-642-13923-9_14

Lukasik, S., Kowalski, P. A., Charytanowicz, M., & Kulczycki, P. (2016). Clustering using Flower Pollination Algorithm and Calinski-Harabasz index. In *2016 IEEE Congress on Evolutionary Computation (CEC)* (pp. 2724-2728). IEEE. https://doi.org/10.1109/CEC.2016.7744132

Maestre, G. E., Pino-Ramírez, G., Molero, A. E., Silva, E. R., Zambrano, R., Falque, L., Gamero, M. P., & Sulbarán, T. A. (2002). The Maracaibo Aging Study: population and methodological issues. *Neuroepidemiology*, *21*(4), 194-201. https://doi.org/10.1159/000059524

Maestre, G. E., Mena, L. J., Melgarejo, J. D., Aguirre-Acevedo, D. C., Pino-Ramírez, G., Urribarrí, M., Chacon, I. J., Chavez, C. A., Falque-Madrid, L., Gaona, C. A., Terwilliger, J. D., Lee, J. H., Scarmeas, N., & Scarmeas, N. (2018). Incidence of dementia in elderly Latin Americans: Results of the Maracaibo Aging Study. *Alzheimer's & Dementia, 14*(2), 140–147. https://doi.org/10.1016/j.jalz.2017.06.2636

Manta, E., Thomopoulos, C., Kariori, M., Polyzos, D., Mihas, C., Konstantinidis, D., Farmakis, D., Mancia, G., & Tsioufis, K. (2024). Revisiting cardiovascular benefits of blood pressure reduction in primary and secondary prevention: Focus on targets and residual risk—A systematic review and meta-analysis. *Hypertension, 81*(5), 1076–1086. https://doi.org/10.1161/HYPERTENSIONAHA.123.22610

Marteau, P.-F. (2009). Time warp edit distance with stiffness adjustment for time series matching. *IEEE Transactions on Pattern Analysis and Machine Intelligence, 31*(2), 306–318. https://doi.org/10.1109/TPAMI.2008.76

McLachlan, G. J., & Basford, K. E. (1988). *Mixture models. Inference and applications to clustering.* M. Dekker.

McQueen, J. B. (1967). Some methods of classification and analysis of multivariate observations. In *Proc. of 5th Berkeley Symposium on Math. Stat. and Prob.* (pp. 281-297).

Melgarejo, J. D., Vatcheva, K. P., Mejia-Arango, S., Charisis, S., Patil, D., Mena, L. J., Garcia, A., Alliey-Rodriguez, N., Satizabal, C. L., Chavez, C. A., Gaona, C., Silva, E., Mavarez, R. P., Lee, J. H., Terwilliger, J. D., Blangero, J., Seshadri, S., & Maestre, G. E. (2024). Association of longitudinal changes in 24-h blood pressure level and variability with cognitive decline. *Journal of Hypertension, 42*(11), 1985–1993. https://doi.org/10.1097/HJH.0000000000003824

Mena, L. J., Felix, V. G., Melgarejo, J. D., & Maestre, G. E. (2017). 24-hour blood pressure variability assessed by average real variability: A systematic review and meta-analysis. *Journal of the American Heart Association, 6*(10). https://doi.org/10.1161/JAHA.117.006895

Moore, W. C., Meyers, D. A., Wenzel, S. E., Teague, W. G., Li, H., Li, X., D'Agostino Jr., R., Castro, M., Curran-Everett, D., Fitzpatrick, A. M., Gaston, B., Jarjour, N. N., Sorkness, R., Calhoun, W. J., Chung, K. F., Comhair, S. A. A., Dweik, R. A., Israel, E., Peters, S. P., Busse, W. W., Erzurum, S. C., & Bleecker, E. R. (2010). Identification of asthma phenotypes using cluster analysis in the Severe Asthma Research Program. *American Journal of Respiratory and Critical Care Medicine, 181*(4), 315–323. https://doi.org/10.1164/rccm.200906-0896OC

Mueen, A., & Keogh, E. J. (2016). Extracting optimal performance from dynamic time warping. In *Proceedings of the 22nd ACM SIGKDD International Conference on Knowledge Discovery and Data Mining* (pp. 2129–2130). ACM. https://doi.org/10.1145/2939672.2945383

Myers, C. S., Rabiner, L. R., & Rosenberg, A. E. (1980). Performance tradeoffs in dynamic time warping algorithms for isolated word recognition. *IEEE Transactions on Acoustics, Speech, and Signal Processing, 28*(6), 623–635. https://doi.org/10.1109/TASSP.1980.1163491

Nakagawa, K., Imamura, M., & Yoshida, K. (2019). Stock price prediction using k-medoids clustering with indexing dynamic time warping. *Electronics and Communications in Japan, 102*(2), 3–8. https://doi.org/10.1002/ecj.12140

Ng, A. Y., Jordan, M. I., & Weiss, Y. (2001). On spectral clustering: Analysis and an algorithm. In T. Dietterich, S. Becker, & Z. Ghahramani (Eds.), *Advances in neural information processing systems*, *14*.

Niako, N., Melgarejo, J. D., Maestre, G. E., & Vatcheva, K. P. (2024). Effects of missing data imputation methods on univariate blood pressure time series data analysis and forecasting with ARIMA and LSTM. *BMC Medical Research Methodology, 24*, 320. https://doi.org/10.1186/s12874-024-02448-3

Ntalianis, E., Cauwenberghs, N., Sabovčik, F., Santana, E., Haddad, F., Claus, P. & Kuznetsova, T. (2023). Feature-based clustering of the left ventricular strain curve for cardiovascular risk stratification in the general population. *Frontiers in Cardiovascular Medicine, 10*. https://doi.org/10.3389/fcvm.2023.1263301

Pallares Robles, A., ten Cate, V., Lenz, M., Schulz, A., Prochaska, J. H., Rapp, S., Koeck, T., Leineweber, K., Heitmeier, S., Opitz, C. F., Held, M., Espinola-Klein, C., Lackner, K. J., Munzel, T., Konstantinides, S. V., ten Cate-Hoek, A., ten Cate, H., & Wild, P. S. (2023). Unsupervised clustering of venous thromboembolism patients by clinical features at presentation identifies novel endotypes that improve prognostic stratification. *Thrombosis Research, 227*, 71–81. https://doi.org/10.1016/j.thromres.2023.04.023

Paparrizos, J., Yang, F., & Li, H. (2024a). Bridging the gap: A decade review of time-series clustering methods. *arXiv preprint*. https://doi.org/10.48550/arXiv.2412.20582

Paparrizos, J., Li, H., Yang, F., Wu, K., d'Hondt, J. E., & Papapetrou, O. (2024b). A survey on time-series distance measures. *arXiv preprint.* https://doi.org/10.48550/arXiv.2412.20574

Paula, D. P., Lopes, L. J., Mill, J. G., Fonseca, M. J. M., & Griep, R. H. (2020). Identifying patterns of diurnal blood pressure variation among ELSA-Brasil participants. *Journal of Clinical Hypertension, 22*(12), 2315–2324. https://doi.org/10.1111/jch.14066

Petitjean, F., Ketterlin, A., & Gançarski, P. (2011). A global averaging method for dynamic time warping, with applications to clustering. *Pattern Recognition, 44*(3), 678–693. https://doi.org/10.1016/j.patcog.2010.09.013

Philips, R. T., Torrisi, S. J., Gorka, A. X., Grillon, C., & Ernst, M. (2022). Dynamic time warping identifies functionally distinct fMRI resting state cortical networks specific to VTA and SNc: A proof of concept. *Cerebral Cortex, 32*(6), 1142-1151. https://doi.org/10.1093/cercor/bhab273

Ratanamahatana, C. A., & Keogh, E. (2004). Everything you know about dynamic time warping is wrong. In *Proceedings of the 3rd workshop on mining temporal and sequential data* (Vol. 32, pp. 1-11). Seattle: Citeseer.

Rodríguez, M. J., del Pozo, F., Arredondo, M. T., Gómez, E. J., & Palma, J. L. (1992). A new method to classify blood pressure time series. In *Proceedings of the 14th Annual International Conference of the IEEE Engineering in Medicine and Biology Society* (pp. 745–747). IEEE. https://doi.org/10.1109/IEMBS.1992.5761199

Sakoe, H., & Chiba, S. (1978). Dynamic programming algorithm optimization for spoken word recognition. *IEEE Transactions on Acoustics, Speech, and Signal Processing, 26*(1), 43–49. https://doi.org/10.1109/TASSP.1978.1163055

Salgado, C. M., Ferreira, M. C., & Vieira, S. M. (2017). Mixed fuzzy clustering for misaligned time series. *IEEE Transactions on Fuzzy Systems, 25*(6), 1777–1792. https://doi.org/10.1109/TFUZZ.2016.2633375

Sardá-Espinosa, A. (2019). Time-series clustering in R using the dtwclust package. *The R Journal, 11*(1), 22–43.

Scherzer, R., Shah, S. J., Secemsky, E., Butler, J., Grunfeld, C., Shlipak, M. G. & Hsue, P. Y. (2018). Association of biomarker clusters with cardiac phenotypes and mortality in patients with HIV infection. *Circulation: Heart Failure, 11*(4). https://doi.org/10.1161/CIRCHEARTFAILURE.117.004312

Schutte, A. E., Kollias, A., & Stergiou, G. S. (2022). Blood pressure and its variability: Classic and novel measurement techniques. *Nature Reviews Cardiology, 19*(10), 643–654. https://doi.org/10.1038/s41569-022-00690-0

Sible, I. J., & Nation, D. A. (2024). 24-hour blood pressure variability via ambulatory monitoring and risk for probable dementia in the SPRINT trial. *The Journal of Prevention of Alzheimer's Disease, 11*(3), 684–692. https://doi.org/10.14283/jpad.2024.35

Spatz, E. S., Martinez-Brockman, J. L., Tessier-Sherman, B., Mortazavi, B., Roy, B., Schwartz, J. I., Nazario, C. M., Maharaj, R., Nunez, M., Adams, O. P., & Nunez-Smith, M. (2019). Phenotypes of hypertensive ambulatory blood pressure patterns: Design and rationale of the ECHORN Hypertension Study. *Ethnicity & Disease, 29*(4), 535–544. https://doi.org/10.18865/ed.29.4.535

Staplin, N., de la Sierra, A., Ruilope, L. M., Emberson, J. R., Vinyoles, E., Gorostidi, M., Ruiz-Hurtado, G., Segura, J., Baigent, C., & Williams, B. (2023). Relationship between clinic and ambulatory blood pressure and mortality: An observational cohort study in 59,124 patients. *The Lancet, 401*(10392), 2041–2050. https://doi.org/10.1016/S0140-6736(23)00733-X

Sun, F. (2023). The impact of blood pressure variability on cognition: Current limitations and new advances. *Journal of Hypertension, 41*(6), 888–905. https://doi.org/10.1097/HJH.0000000000003422

Tan, C. W., Petitjean, F., Keogh, E., & Webb, G. I. (2023). Assessing similarity under dynamic time warping between time series that differ in length. *Available at SSRN.* https://dx.doi.org/10.2139/ssrn.4349264

Tan, C. W., Petitjean, F., & Webb, G. I. (2020). FastEE: Fast ensembles of elastic distances for time series classification. *Data Mining and Knowledge Discovery, 34*(1), 231–272. https://doi.org/10.1007/s10618-019-00663-x

Vargas, T. M. (2023). *A machine learning approach to obese-inflammatory phenotyping* (Master's thesis, The University of Texas Rio Grande Valley). ProQuest Dissertations Publishing.

Vázquez, I., Villar, J. R., Sedano, J., & Simić, S. (2021). A comparison of multivariate time series clustering methods. In Á. Herrero, C. Cambra, D. Urda, J. Sedano, H. Quintian, & E. Corchado (Eds.), *SOCO 2020: 15th International Conference on Soft Computing Models in Industrial and Environmental Applications* (pp. 571–579). Springer. https://doi.org/10.1007/978-3-030-57802-2_55

Wagner, R. A., & Fischer, M. J. (1974). The string-to-string correction problem. *Journal of the Association for Computing Machinery, 21*(1), 168–173. https://doi.org/10.1145/321796.321811

Wang, F., Zhou, J., Tian, Y., Wang, Y., Zhang, P., Chen, J. & Li, J. (2018). Intradialytic blood pressure pattern recognition based on density peak clustering. *Journal of Biomedical Informatics, 83*, 33–39. https://doi.org/10.1016/j.jbi.2018.05.013

Wang, X., Smith, K., & Hyndman, R. (2006). Characteristic-based clustering for time series data. *Data Mining and Knowledge Discovery, 13*(3), 335–364. https://doi.org/10.1007/s10618-005-0039-x

Ward Jr, J. H. (1963). Hierarchical grouping to optimize an objective function. *Journal of the American Statistical Association*, *58*(301), 236-244. https://doi.org/10.2307/2282967

Whelton, P. K., Carey, R. M., Aronow, W. S., Casey, D. E., Collins, K. J., Dennison Himmelfarb, C., DePalma, S. M., Gidding, S., Jamerson, K. A., Jones, D. W., MacLaughlin, E. J., Muntner, P., Ovbiagele, B., Smith, S. C., Spencer, C. C., Stafford, R. S., Taler, S. J., Thomas, R. J., Williams, K. A., Williamson, J. D., & Wright, J. T., Jr. (2018). 2017 ACC/AHA/AAPA/ABC/ACPM/AGS/APhA/ASH/ASPC/NMA/PCNA guideline for the prevention, detection, evaluation, and management of high blood pressure in adults: A report of the American College of Cardiology/American Heart Association Task Force on Clinical Practice Guidelines. *Hypertension, 71*(6), e13–e115. https://doi.org/10.1161/HYP.0000000000000066

Xu, J., Jiang, F., Wang, A., Zhi, H., Gao, Y., Tian, J., Mo, J., Chen, Z., Xu, A.-D., Luo, B., Hu, B., Zhang, Y., Zhao, X., Wang, Y., Li, H., Shen, H., & Wang, Y. (2021). Ambulatory blood pressure profile and stroke recurrence. *Stroke & Vascular Neurology, 6*(1). https://svn.bmj.com/content/6/3/352

Yang, W.-Y., Melgarejo, J. D., Thijs, L., Zhang, Z.-Y., Boggia, J., Wei, F.-F., Hansen, T. W., Asayama, K., Ohkubo, T., Jeppesen, J., Dolan, E., Stolarz-Skrzypek, K., Malyutina, S.,

Casiglia, E., Lind, L., Filipofsky, J., Maestre, G. M., Li, Y., Wang, J.G., … Staessen, J. A. (2019). Association of office and ambulatory blood pressure with mortality and cardiovascular outcomes. *JAMA, 322*(5), 409–420. https://doi.org/10.1001/jama.2019.9811

Yim, O., & Ramdeen, K. T. (2015). Hierarchical cluster analysis: comparison of three linkage measures and application to psychological data. *The quantitative methods for psychology,* 11(1), 8-21. https://doi.org/10.20982/tqmp.11.1.p008

Zakaria, J., Mueen, A., & Keogh, E. (2012). Clustering time series using unsupervised-shapelets. In M. J. Zaki, A. Siebes, J. Xu Yu, B. Goethals, G. Webb, X. Wu (Eds.), *Proceedings of the 2012 IEEE 12th International Conference on Data Mining* (pp. 785–794). IEEE. https://doi.org/10.1109/ICDM21070.2012

Zhang, N., & Sun, S. (2023). Multiview unsupervised shapelet learning for multivariate time series clustering. *IEEE Transactions on Pattern Analysis and Machine Intelligence, 45*(4), 4981–4996. https://doi.org/10.1109/TPAMI.2022.3198411

Zhu, Y., Chen, X., Geng, S., Li, Q., Yuan, H., Zhou, X., Li, H., Li, J., & Jiang, H. (2020). Association between ambulatory blood pressure variability and frailty among older hypertensive patients. *Journal of Clinical Hypertension, 22*(9), 1703–1712. https://doi.org/10.1111/jch.13986

Zumer, J. (2023). *pytwed: Python implementation of Time Warp Edit Distance (TWED)* [Source code]. GitHub. https://github.com/jzumer/pytwed

VITA

John Knight graduated from the University of Texas Rio Grande Valley with a Bachelor of Science in Statistics in May 2023. He earned his Master of Science in Applied Statistics and Data Science, also at the University of Texas Rio Grande Valley, in December 2025. He can be contacted via email at knightjohn2@gmail.com.